

INTEGRATION OF MULTISENSOR AIRBORNE DATA FOR AN OBJECT BASED
SPECTRAL CLASSIFICATION

by

Roger Stephen
BSc, University of Victoria, 2004

A Thesis Submitted in Partial Fulfillment
of the Requirements for the Degree of

MASTER OF SCIENCE

in the Department of Geography

© Roger Stephen, 2014
University of Victoria

All rights reserved. This thesis may not be reproduced in whole or in part, by photocopy
or other means, without the permission of the author.

Supervisory Committee

INTEGRATION OF MULTISENSOR AIRBORNE DATA FOR AN OBJECT BASED SPECTRAL CLASSIFICATION

by

Roger Stephen
BSc, University of Victoria, 2004

Supervisory Committee

Dr. Knut Olaf Niemann (Department of Geography)
Supervisor

Dr. Trisalyn Nelson (Department of Geography)
Departmental Member

Abstract

Supervisory Committee

Dr. Knut Olaf Niemann (Department of Geography)
Supervisor

Dr. Trisalyn Nelson (Department of Geography)
Departmental Member

Integration of multisensor airborne data for object based image analysis, and spectral classification of individual trees is complicated by the multi-modal operation of complimentary sensors required for intersensor calibration. Simplified and generalized representations of sensor data impacts the ability to calibrate, rectify, segment, and extract scene objects represented as differing scales. This research project examines the effect and implications of using lidar to calibrate, and rectify airborne imaging spectrometer to an appropriate resolution digital surface model. Through the use of a normalized digital canopy surface model, tree objects are detected and integrated with field surveyed species data for trees of classification interest. Canopy structure is used to segment, and extract airborne imaging spectrometer data for assessment and suitability in species classification.

Table of Contents

Supervisory Committee	ii
Abstract	iii
Table of Contents	iv
List of Tables	vi
List of Figures	vii
Acknowledgments.....	viii
Dedication	ix
Chapter 1 - Introduction.....	1
1.1 Introduction.....	1
1.2 MAP Series Overview	3
1.3 Acquisition and Study Site overview.....	3
1.3.1 King Island Study Site	3
1.3.2 Pack Lake Study Site	5
1.4 Research Questions and Associated Objectives	6
1.5 Thesis Structure	6
Chapter 2 – Acquisition, Calibration and Pre-processing.....	8
2.1 Introduction to Acquisition/Processing/Calibration	8
2.2 Multisensor Airborne Platform Series	8
2.2.1 Inertial Navigation System	9
2.2.2 LIDAR system	9
2.2.3 Digital Frame Camera.....	10
2.2.4 Aisa Eaglet.....	10
2.2.5 Aisa Eagle	12
2.3 Radiometric Calibration / Atmospheric Correction	13
2.4 Digital Surface Model for Rectification	14
2.5 INS Trajectory and Integration	18
2.6 Boresight Calibration	21
2.7 Direct Georeferencing / Orthorectification	23
Chapter 3 – Tree Object Representation, Feature Extraction and Classification	25
3.1 Introduction.....	25
3.2 Point Cloud Normalization	28
3.3 Canopy Height Model Gridding	30
3.4 Individual Tree Top Detection.....	30
3.5 Individual Tree Crown Delineation	31
3.6 Spectral Extraction.....	33
3.6.1 Field Survey Data – Collection and Assessment	33
3.6.2 Training Database Spectral Extraction – King Island.....	35
3.6.3 Training Database Spectral Extraction – Pack Lake.....	38
3.7 Classification.....	40
3.7.1 Spectral Angle Mapper	40

3.7.2 Individual Tree stem based classification – King Island	41
3.7.3 Crown Based spectral classification – Pack Lake.....	42
3.8 Results.....	42
3.8.1 King Island Individual Tree based SAM Classification Results	42
3.8.2 Pack Lake Crown based SAM Results	46
Chapter 4 – Discussion and Future Work.....	48
Bibliography	53
Appendix A List of Abbreviations.....	56

List of Tables

Table 1. Tree top Search Kernel and Associated Height Range.....	30
Table 2. ITC Stopping Rules	32
Table 3. King Island Field Surveyed Stems Training Data Distribution	35
Table 4. Pack Lake Training Species Distribution	38
Table 5. Species Average Spectra SAM Confusion Matrix	43
Table 6. Full Range Multi-Endmember SAM Confusion Matrix.....	44
Table 7. Spectral Subset Multi-Endmember SAM Confusion Matrix.....	45
Table 8. Pack Lake SAM Confusion Matrix	46

List of Figures

Figure 1. King Island Digital Surface Model	4
Figure 2. King Island Canopy Height Model.....	4
Figure 3. Eaglet trajectory and 58.55° wide field of view in the across track dimension	11
Figure 4. Example of shifted feature spectral representation due to inappropriate DSM applied during the direct-georeferencing process.	15
Figure 5. Lidar point cloud cross section and max-z DSM gridding representation	17
Figure 6. Raw AIS Flightline depicted as a sequential time series.....	18
Figure 7. IMU Orientation Reference Frame (reproduced from Muller <i>et al.</i> 2002 p.3) .	19
Figure 8. Effect of poor time synchronizaton between INS and AIS	20
Figure 9. Synchronized Raw Image with roll attitude plotted in blue line	21
Figure 10. Effect of AIS Boresight Missalignment Angle on uncalibrated flightlines	22
Figure 11. Processing Flowchart.....	28
Figure 12. Point Cloud Normalization.....	29
Figure 13. Species Average Reflectance	36
Figure 14. Averaged Species Standard Deviation.....	37
Figure 15. Averaged Species Spectra- Coefficient of Variation.....	37
Figure 16. Spectral Angle Example	41

Acknowledgments

This thesis project has been part of a long and extended graduate program that has provided me with a unique opportunity to be involved in applied remote sensing, ranging from acquisition, field sampling, calibration, pre-processing, data integration and application development. I owe a huge amount of gratitude to my supervisor Dr. Olaf Niemann for the kind, encouraging support during my research projects. I am proud to have been associated, and to continue to research with the Hyperspectral & Lidar Research Group. There is something so rewarding about waking up and wanting to get to work on the problem that you did not want to leave the evening before. Geoff, Diana, Ben, Astrid, Georgia, and Rafael; you all have been part of what makes this place so great to do applied remote sensing research. I feel an especially warm thank you belongs to Fabio Visintini, a close colleague and friend whom I have spent numerous hours discussing remote sensing theory, the finer parts of Italy, and humanity with; you have been a most loyal friend and contributed greatly through education and encouragement over many years. I would like to acknowledge the opportunities for research provided by Jon Corbett, Rosaline Canessa, Steve Bloomer and Darwin Monita, each of you took risks with me and opened up amazing opportunities for me. I have been very fortunate for the support provided by my close family and friends who have always supported my dreams. Thank you to Mum, Dad, Alice, Ken, David, Tammy, and Jill. I would like to acknowledge the support of Strategic Forest Management, and Terra Remote Sensing. Rick, Dave, Ted, Taylor, Yuna, and Ian thank you for the ongoing support both in and out of the office. Finally, I want to acknowledge a man who I did not get to know well enough, but for years was intrinsically involved in the acquisition of airborne data I work with on a daily basis; rest in peace Jim.

Dedication

This thesis is dedicated to my late grandparents Cedric, Mary, James, and Rebecca. Each of these fine role models supported me from a young age and instilled a love for science and our natural environment.

Chapter 1 - Introduction

1.1 Introduction

Increased spatial resolution of Airborne Imaging Spectrometers (AIS) on the order of 0.5-1.5m provides a unique opportunity to address influences of variations in signal-to-noise ratios (S/N) prevalent within specific objects and its effect on classification and feature extraction. One such analytical framework involves the definition and use of Individual Tree Crown (ITC) objects. ITC objects are vector representations of an individual tree crown, either as a point based object, or as polygon based object, representing the tree crown as projected onto a ground surface.

The detection of ITCs is well established within the remote sensing literature, with initial studies of passive optical imagery examining the relationship between high reflectance at the apex of a crown, and detection using local maxima filters (D. G. Leckie et al., 2005; Niemann, Adams, & Hay, 1998; Wulder, Niemann, & Goodenough, 2000). Successful detection of ITCs is related to the spatial resolution of the image used to detect them, and the scale and size of the ITCs as scene objects. A remote sensing scene model that contains objects that are larger than the image resolution is considered an H-resolution model, while an image resolution that is larger than the objects of interest is considered an L-resolution model (Strahler, Woodcock, & Smith, 1986). ITC objects that are relatively small compared to the pixel resolution of the image present an L-resolution model and can contribute to errors of omission, as the local maxima detected potentially represents a cluster of trees. For the same image resolution, ITCs of a comparatively larger size are represented by multiple image pixels, an H-resolution model, and tend to have higher detection rates; however they can suffer due to errors of commission, due to multiple local maxima being detected. The passive optical detection algorithms used for ITCs have been successfully extended into studies of Airborne Lidar Scanner (ALS) derived rasters and provide similar detection capacities (D. Leckie et al., 2003). ITCs detected from ALS data can be used to produce vector representations of crowns based on their structure, useful as segmentation objects in Object Based Image Analysis (OBIA). Object based segmentation of individual tree crowns provides a mechanism to

reduce noise from adjacent image spectra by removing them from analysis; effectively increasing the signal to noise ratio, and reducing spectral variance. The ability to extract object specific and appropriate spectral information for an ITC is directly related to the spatial resolution of the ALS and AIS data. The resolution of ALS data has a direct impact on the ability to detect ITC scene objects; when this resolution is poorly matched to the AIS and imagery is segmented, the resulting ITC spectra will not represent the object appropriately. Inappropriate spectral segmentation adds noise to ITC objects potentially causing problems for subsequent classifications.

The projects presented in this thesis take advantage of H-resolution ALS data appropriate in resolution for ITC object detection and AIS segmentation. This OBIA based analysis enables within ITC spectral extraction for evaluation of species based classification.

Given the reliance on the use of both form and function through lidar and hyperspectral data, within-crown ITC spectral sampling must be supported through the close integration of onboard sensors, from acquisition to final spectral sampling. This thesis examines the end-to-end integration of multisensory data through the use of two TRSI/UVic Multisensor Airborne Platforms (MAP). Examples of two specific forest surveys are used to illustrate the sensor integration, object definition and subject analysis. Both of these surveys include discrete return lidar, VNIR hyperspectral data, and orthophotography. The Lidar surveys have point density sufficient to support image calibration, and were used to generate a top of reflective canopy Digital Surface Model (DSM) for hyperspectral orthorectification, and object definition to support spectral extraction. High spatial resolution imaging spectrometer data, by its very nature provides both enhanced opportunities for object based spectral extraction, and combined with high-resolution lidar based raster models; enable assessment and validation of both the calibration and rectification process. The following sections describe the acquisition, processing, rectification, and validation of AIS flightlines collected using the TRSI/UVic MAP-series integrated sensor platforms.

1.2 MAP Series Overview

The TRSI / UVic MAP platforms are highly integrated remote sensing platforms that are designed to support an onboard hyperspectral AIS with adjacently mounted discrete multi return ALS, Inertial Navigation System (INS) and a high resolution digital frame camera. Utilizing a common airframe and almost identical acquisition geometry, the ALS provides multiple co-registered lidar returns in the form of a point cloud enabling three-dimensional positional information coincident to the Instantaneous Field of View (IFOV) of each rectified AIS pixel. Mounting the sensors on the same rigid platform allows an INS derived, single platform trajectory and error budget to be shared for direct georeferencing of ALS, AIS, and digital frame camera. Simultaneous collection of sensor data ensures that structural information measured using the ALS is temporally consistent and relevant for rectification of the optical data collected by the AIS and frame camera.

1.3 Acquisition and Study Site overview

This thesis examines two study sites located on the mid-coast of British Columbia. The first site is located on southern portion of King Island; the second study site is Pack Lake. Both sites are dominated by coastal coniferous forests and mountainous coastal terrain. The King Island site was surveyed using the MAP-2 a lightweight rotary platform system, while the Pack Lake Sound site was surveyed using the MAP-1 surveyed from a fixed wing aircraft. The main difference between the two platforms is the low weight and compact nature of the MAP-2 and its capability to image at a higher spatial resolution than the MAP-1, based on its ability for slow speed, high frame rate acquisition at a low altitude. Further details on the MAP series integrated sensor platforms is found in the calibration and rectification chapter.

1.3.1 King Island Study Site

The King Island study site ($51^{\circ} 57' N$, $127^{\circ} 52' W$), is located on the central coast of British Columbia at the north end of Fitz Hugh Sound. The study site, and area imaged

for the survey occupy approximately 8000 hectares on the southern portion of the island. The site elevation ranges from 0-645m above sea level, characterized by steep slopes, and multiple watersheds crossing the acquisition area (Figure 1).

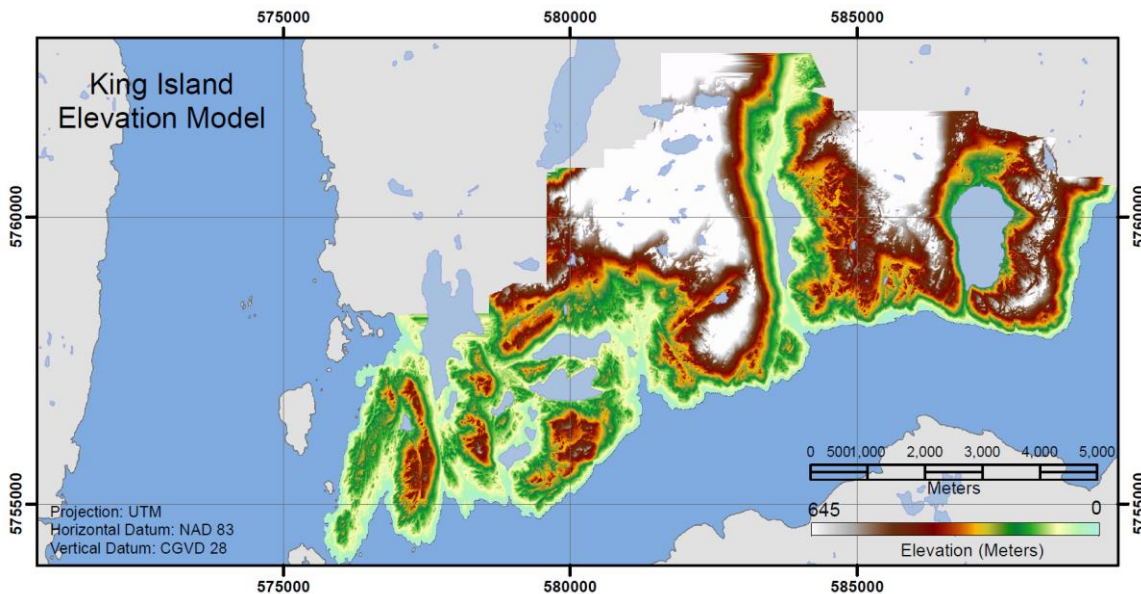


Figure 1. King Island Digital Surface Model

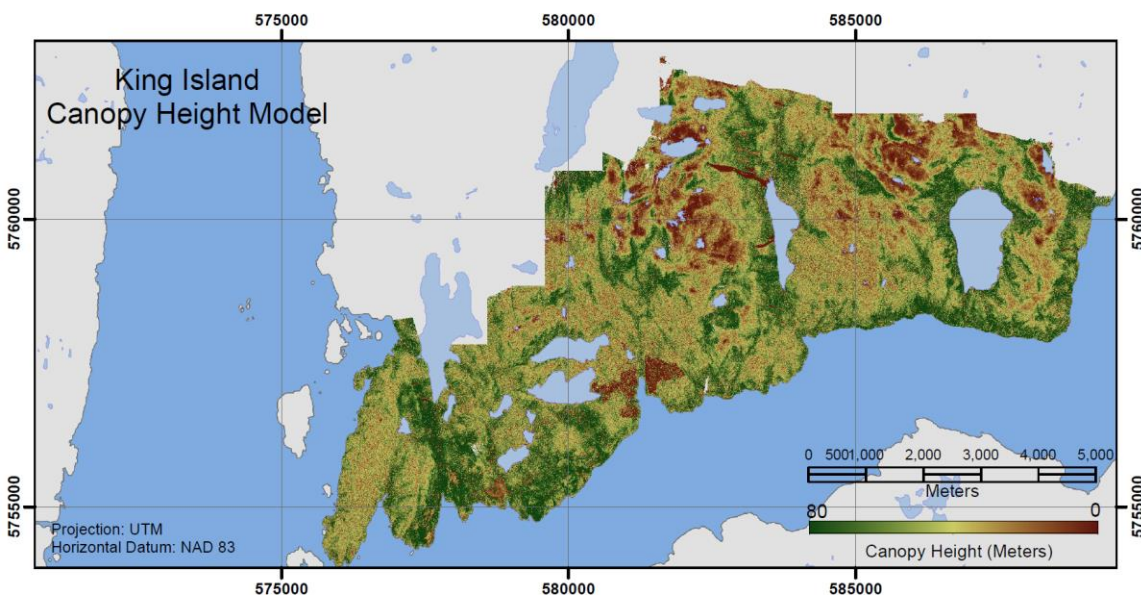


Figure 2. King Island Canopy Height Model

The King Island study site is dominated by Western red cedar, with co-dominant Western hemlock and Amabilis fir. In addition patches of Sitka spruce and Mountain hemlock also grow within the study area. The Canopy Height Model (CHM) depicted in Figure 2. depicts canopies up to 80m in height and provides an indication of areas where old growth stands dominate the study site.

The site was surveyed on July 16th 2010 between 11:50 and 14:00 Pacific Standard Time, acquired at this time of day to minimize bidirectional reflectance. Using the MAP-2 sensor cluster, a total of 29 flightlines were surveyed utilizing a Bell 206B Jet Ranger rotary platform. Each flightline consisted of coincident, and concurrent, discrete multi-return lidar, VNIR hyperspectral, digital frame camera images, and platform position and orientation information as collected by the INS. The use of a rotary platform for this survey was necessary to follow the complex terrain at a relatively constant above ground elevation, while at the same time maintain a stable over ground platform velocity. A fixed wing platform is unable to dynamically follow the underlying terrain with the result being large magnitude shifts in field of view while moving over highly variable terrain as found in the study site.

1.3.2 Pack Lake Study Site

The Pack Lake Study site (51° 10' 30" N, 127° 32' 30" W), is located on the central coast of British Columbia, north of Mereworth Sound. The study site and area imaged for this project occupy approximately 14,000 hectares of forested land surrounding the lake. The site elevation ranges from 0-600m above sea level and is characterized by the north side of the lake with a southern aspect and an area south of the lake with a North facing aspect. The study site is dominated by Western red cedar, being the leading species for most of the acquisition area. Mountain hemlock, Western hemlock, Amabilis fir and Sitka Spruce are found throughout the acquisition site with Red alder located in many of the riparian areas.

The site was imaged on August 16th, 2012 between 11:30 and 14:00 Pacific Standard Time, the acquisition was acquired at this time to take advantage of solar illumination

geometry and to minimize bi-directional reflectance. The area was surveyed with the MAP-1 sensor cluster mounted on a Piper Navajo airframe, flying in an alternating East/West acquisition pattern imaging a total of 20 overlapping flightlines.

1.4 Research Questions and Associated Objectives

The overall objective of this thesis is to examine the integration of multisensor airborne data utilizing an object oriented spectral classification for individual trees. Two main research questions guide this research.

- 1) What are the geometric effects to raw imagery of survey parameters, calibration, and rectification in terms of data representation before spectral sampling?

- 2) Can Airborne Imaging Spectrometer spectra be classified at a species level using the Spectral Angle Mapper Algorithm?

Based on the research questions, the objectives are as follows:

- 1) To examine the end to end processing methodology and examine best practices to ensure data integrity and spatial consistency between raw lidar point data, the lidar derived raster models supporting calibration, rectification and segmentation of coincident hyperspectral.

- 2) To integrate field surveyed stem positions for spectral extraction, evaluation, classification and accuracy assessment.

1.5 Thesis Structure

This thesis is based on 4 chapters that utilize a systems approach to investigate the fusion of multisensor AIS data for object based, individual stem based spectral classification. The first chapter provides an introduction and background to the project, the integrated

MAP series sensor cluster and the research motivations. The second chapter is a detailed examination of the project study sites, sensor hardware, configuration, and characteristics and the data streams acquired. AIS radiometric and geometric calibration and rectification are discussed at the end of chapter two. The third chapter details the OBIA approach utilized for feature representation, extraction, integration and classification. Results are presented at the end of the third chapter. The final chapter is used to discuss the results and future potential research in this field.

Chapter 2 – Acquisition, Calibration and Pre-processing

2.1 Introduction to Acquisition/Processing/Calibration

The purpose of this chapter is to provide background information on how AIS imagery was acquired, calibrated, and georeferenced utilizing complimentary and concurrently collected INS trajectory, and ALS derived raster models. This background information is provided so that the reader is made aware of how independent sensors and their data streams are integrated, how this affects AIS feature representation, extraction, and positional accuracy of georeferenced pixels.

The first part of this chapter provides an overview of the MAP series onboard sensors, including INS, ALS, AIS and digital frame camera, and how sensor characteristics and configuration relate to the two study sites. The next section describes how the onboard INS, and ALS data were integrated and calibrated to determine AIS sensor position and orientation, necessary for the direct georeferencing of image pixels as determined through ray tracing and intersection with an ALS derived DSM.

2.2 Multisensor Airborne Platform Series

The Multisensor Airborne Platform (MAP) series refers to two separate (MAP-1 and MAP-2) integrated systems for combined ALS, AIS, and digital orthophoto acquisition. Sensors are physically clustered together with minimized lever arm offsets and angular misalignment, enabling coincident and complimentary ALS measured point clouds for direct georeferencing and orthorectification of imagery data. The use of a strapdown INS provides synchronized position and orientation of the platform, relating unique acquisition geometry to each sensor through lever arm offsets and boresight calibration. The MAP-1 is the first generation of the series and at the time of this study encompassed an Applanix POS AV 510 INS, a Nikon D3 camera, a Specim AISA (Airborne Imaging

Spectrometer for Applications) Dual VNIR/SWIR AIS, and a multi-return discrete lidar system. The MAP-1 is flown utilizing a fixed wing Piper Navajo by Terra Remote Sensing, based out of Sidney B.C. The MAP-2 is a lightweight version of the MAP-1 and was specifically designed for a rotary platform and utilizes an Applanix POS AV 410, Nikon D3 camera, and a Specim AISA Eaglet VNIR sensor. The Map-2 system flown on a Bell Jet Ranger platform is capable of low altitude high resolution surveys over complex terrain common place on the British Columbia coast. The ability to acquire complementary multisensor data concurrently enables cost effective surveys with appropriate data for post survey data fusion. In the following sections a detailed description of the hardware and configuration will be discussed.

2.2.1 Inertial Navigation System

The INS used for the King Island survey is the POS A/V 410, while for Pack Lake the system used is a POS A/V 510. The Applanix POS A/V is an integrated hardware and software system consisting of GPS hardware for positioning, and a strapdown INS for determining orientation. The INS is essential for providing a high frequency navigation and orientation solution for the platform and through the use of colinearity enabling direct georeferencing of time synchronized sensor measurements. The main difference between the POS A/V 410 and 510 are in terms of the absolute angular accuracy in terms of roll, pitch, and heading with the POS/AV 510 having the best obtainable absolute accuracy (Mostafa, 2001).

2.2.2 LIDAR system

The ALS system used for both the King Island and Pack Lake study site is a discrete multi-return lidar. The ALS is an active sensor capable of calculating distance between the sensor and the surface objects through the precise timing of emitted and received pulses of electromagnetic energy emitted at 1064nm. The pulse repetition frequency for the ALS was up to 150 kHz and was dependent on acquisition elevation. For each emitted pulse, up to three returns were detected from the incoming returned energy designated as first, intermediate and last return. The beam divergence for the pulse was 0.009° , with an

overall scan angle of 26° using an oscillating mirror to cover the scan pattern. The radiometric resolution of the intensity data was digitized at 14 bits. To minimize boresight misalignment, the IMU is mounted directly to the top face of the ALS, effectively capable of modeling orientation of the ALS principle point. Direct georeferencing utilizing lever arm offset GPS position and orientation from the IMU enable accurate positioning of lidar returns.

2.2.3 Digital Frame Camera

Digital aerial photographs were imaged with a Nikon D3X full frame 35mm camera. The D3X utilizes a Complementary Metal Oxide Semiconductor (CMOS) sensor consisting of a detector array of 6048×4032 elements measuring $5.95 \mu\text{m}$. Strobe triggered frames were acquired encoding GPS timing information for each frame to enable synchronization with INS trajectory for direct georeferencing and orthorectification. Final orthorectified images were output at a 0.25m spatial resolution.

2.2.4 Aisa Eaglet

The Aisa Eaglet, a VNIR hyperspectral AIS, was configured to record 212 spectral bands between the range of 396-1004nm. While 848 spectral bands are available for use on the Charge Coupled Device (CCD), this was reduced by spectrally binning by a factor of four. Spectral binning has been used to increase the SNR from features of interest (Davis et al., 2002) and was used in this project to increase the SNR. The average sampling interval for this spectral range was 2.88nm . The Eaglet AIS utilizes a lens with a field of view of 58.55° , a focal length of 10.56mm , with CCD detector pixels measuring $7.4 \mu\text{m}$. The detector array consists of 1600 spatial pixels that were binned spatially twice to produce 800 image pixels. In 2x spatial binning mode the effective detector pixel size becomes $14.8 \mu\text{m}$ enabling a Horizontal Instantaneous Field of View (HIFOV) of 0.083° .

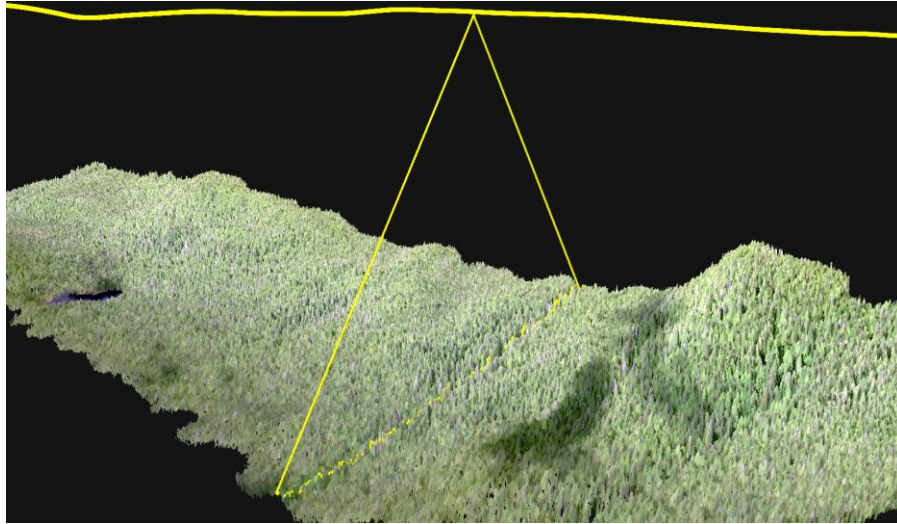


Figure 3. Eaglet trajectory and 58.55° wide field of view in the across track dimension

A major consideration of this project was the collection of high spatial resolution images in a difficult to survey mountainous terrain, where a rotary platform was the only practical option. A nominal ground sampling distance (GSD) of 0.5m pixels was planned for this project, however in practice maintaining a square pixel dimension is impossible. The dimensions of pushbroom AIS pixels at acquisition represent differing along and across track geometries determined by the above ground acquisition elevation the frame rate, and the acquisition elevation. To achieve a nominal GSD of 0.5m, the frame rate was set to image at 40Hz while acquisition velocity was maintained as close to 20m/s as possible. To maintain approximately square pixels, acquisition elevation was maintained close to 500m above the ground level (AGL) throughout the survey, however based on very complex terrain this was not always possible resulting in slight changes in the ground sampled for each pixel.

$$IFOV = 2 * \tan^{-1} \left(\frac{d}{2f} \right)$$

$$IFOV \text{ unbinned} = 0.0402^\circ$$

$$IFOV \text{ 2x binning} = 0.0803^\circ$$

Equation 1. Instantaneous Field of View Calculation

The determination of a nominal GSD value for the project was based on a combination of sensor parameters, acquisition conditions and project goals. The IFOV of the sensor and acquisition height is the primary consideration in determining the across track dimension of ground pixels imaged by the sensor. While it would have been possible to acquire higher resolution spatial pixels in a spatially unbinned mode this would necessitate a 50% reduction in platform velocity in addition to a loss in SNR. The across track pixel size of a ground pixel at ~400m AGL is 0.5m. To match the same along track dimension and have square pixels at a frame rate of 40Hz, it was necessary to image at an over ground velocity of 20m/s. The integration time of the sensor for the King Island study areas was set at 2ms.

2.2.5 Aisa Eagle

The Aisa Eagle is very similar to the Aisa Eaglet being a VNIR spectrometer with a design that predates the Eaglet. The Eagle was configured to record in the spectral range between 392-996nm. A total of 528 spectral bands are available but to increase signal to noise the spectral bands were binned by a factor of four enabling 132 bands. The average sampling interval for this spectral range was 4.5nm. The Eagle AIS has a FOV of 36.76° a focal length of 18.49mm, with CCD detector pixels measuring 12μ . The detector array consists of 1024 spatial pixels of which the first 56 are reserved for a Fibre Optic Downwelling Irradiance Sensor (FODIS). The sensor was configured in 2x Spatial binning mode, this provided 483 pixels in the across track dimension, and doubled the effective detector element to 24μ , this produced an HIFOV of 0.0744° .

Similar to the King Island Eaglet survey, the Airborne Imaging Spectrometer for Applications (AISA) Eagle Pack Lake survey was performed with a goal of capitalizing on spatial resolution and enable individual tree crowns to be sampled with multiple spectra. The limiting factor for this survey was that it utilized a fixed wing Piper Navajo

aircraft with the slowest practical survey speed being 65m/s. While, in theory, it is possible to set a frame rate of 65Hz to attempt and collect 1m pixels in the along track dimension, this frame rate based on past experience creates too much data throughput for the acquisition computer causing dropped frames. To compromise, a frame rate of 43Hz was set for the Pack Lake AISA survey enabling an along track dimension ground sampling distance of 1.5m when flying at a speed of 65m/s. To image pixels with a proportional across track dimension it was necessary to maintain an AGL acquisition elevation of approximately 1155m. The integration time for this survey was set a 7ms.

2.3 Radiometric Calibration / Atmospheric Correction

The Eagle and Eaglet VNIR AIS sensors both use a CCD that digitizes and records a signal proportional to incoming photon energy at each detector element in the form of a 12bit Digital Number (DN). Raw images encoded with DN's are unit less, and need to be calibrated to radiance through a radiometric calibration. Radiometric calibration utilizes a calibration file of gain and offset and a dark current file. The dark current file, collected at the end of each flightline with the shutter closed, provides a measurement of background level DN per detector pixel that needs to be removed from each radiance file before applying the radiance calibration offsets. Regular lab based radiometric calibration of the AISA Eaglet and Eagle sensor utilize an integration sphere with calibration reference lamps to characterize the response of each detector element across each spatial pixel. For each detector pixel a gain (c_1) and offset (c_0) value is calculated and recorded in a calibration file for radiometric pre-processing. After dark current subtraction, the gain and offset calibration file is applied calibrating each pixel to at sensor radiance, L ($\text{mWcm}^{-2} \text{sr}^{-1} \mu\text{m}^{-1}$).

$$L=c_0 + c_1(\text{DN})$$

Equation 2. Equation relating DN to Radiance through calibrated gain and offset.

The transformation of data from DN to units of radiance, L , characterizes the signal strength acquired at each sensor pixel at flight altitude. In order to analyze surface features and objects with spectral techniques relying on spectral shape, data in Reflectance units are required. In this case it was necessary to perform a further radiometric correction to account for the contribution of the atmosphere on the measured signal. In the absence of in-scene calibration targets and field-collected spectra, the atmospheric correction was performed using a radiative transfer code. For the King Island and Pack lake dataset, MODerate Resolution Atmospheric TRANsmission (MODTRAN5) was used to transform the dataset from Radiance to Surface Reflectance.

A Mid-Latitude Summer atmospheric model, with Maritime aerosol profile extinction was selected to characterize the atmosphere. Water vapor column was estimated at approximately 1.3 g/cm^2 , while, based on clear sky conditions and information collected during data acquisition, visibility was estimated at 35 km. MODTRAN was run in radiance mode for each flight-line taking into account the proper viewing and illumination conditions.

2.4 Digital Surface Model for Rectification

The direct georeferencing technique used to reference AIS data relies on a raster based elevation model projected in a local mapping reference frame with orthometric elevations referenced to the same geodetic vertical datum as the position and orientation data modelled from the INS. It is necessary to use a consistent geoid model for the INS trajectory and DSM, as the relative distance between the sensor and elevation model is required ray tracing (Muller & Lehner, 2002).

The use of consistent vertical datum, geoid model, and orthometric elevation between the sensor position and the DSM enable ray tracing between the sensor and the DSM enabling per pixel positioning. The representation and resolution of the digital elevation model has direct implications on the positioning of scan pixels and the ability to orthorectify the data. Low acquisition altitude, wide sensor FOV and high surface relief

all impact the potential for displacement of georeferenced pixels if terrain is not modelled accurately (Muller & Lehner, 2002). For the King Island Eaglet VNIR survey each of the previously mentioned conditions potentially affecting rectification is present. The sensor Field of View (FOV) of 58.55° is wide, acquisition altitude $\sim 400\text{m}$ AGL is low, and relief in the form of both underlying ground terrain, as well as above ground features such as tree canopies, measuring up to 80m , required a very detailed elevation model that represented the top of the reflective surface. A top of reflective surface elevation model, or DSM (Niemann, Frazer, Loos, & Visintini, 2009; Yoon, 2008) is a type of Digital Elevation Model (DEM) that models the top of the canopy and not the underlying topography that has traditionally been used in photogrammetry for image rectification. With tall features such as the trees found in the King Island study site it is very important that a DSM be used not only for AIS direct georeferencing but also rectification to reduce feature displacement (Schlapfer & Richter, 2002; Sheng, Gong, & Biging, 2003; Yoon, 2008).

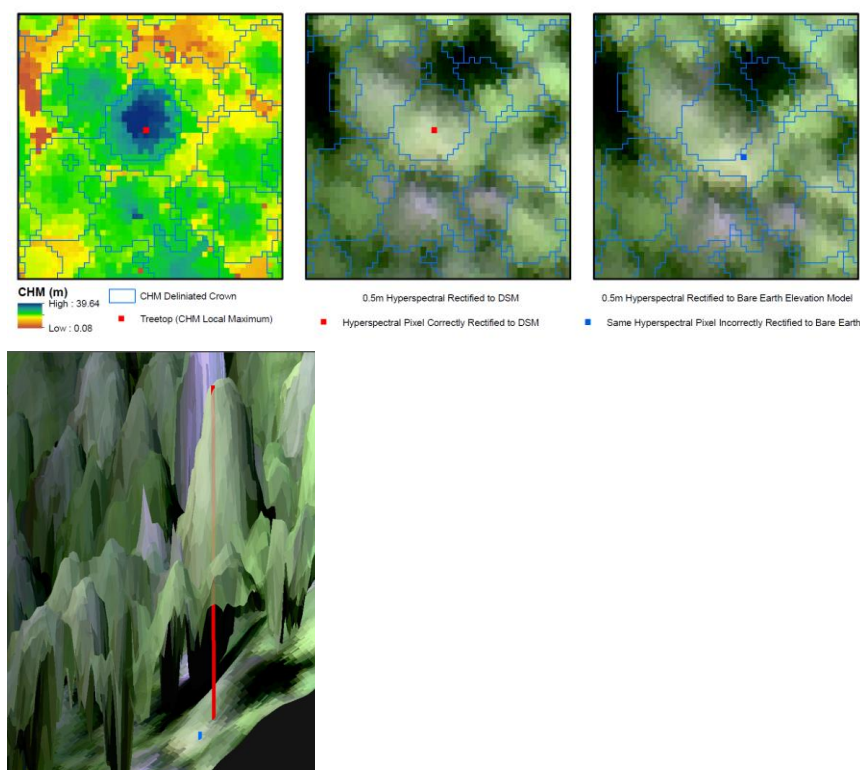


Figure 4. Example of shifted feature spectral representation due to inappropriate DSM applied during the direct-georeferencing process.

The use of a DSM and interrelated lidar derived raster models is integral to the representation, detection, and spectral sampling for object based sampling of trees and their canopies, as well as for the integration of field surveyed tree stem positions required for spectral endmember extraction.

Lidar point clouds were delivered from TRSI in industry standard LAS 1.2 files with points classified into American Society for Photogrammetric Remote Sensing (ASPRS) classes, default (class 1) and ground (class 2). The point density for this project averaged 15 points / square meter and was deemed more than adequate for the creation of a continuous DSM at a 0.5m cell size resolution. A spatial resolution of 0.5m was chosen as it closely matched or was slightly smaller than the GSD based on survey elevation and spatial binning options as suggested by (Muller & Lehner, 2002). To calculate the DSM, the lidar point cloud was first blocked into 1km x 1km tiles, each having a lower left hand origin registered to a whole 1000m interval easting and northing. The tiling scheme was applied for all raster images within the project enabling pixel alignment between images and point features derived from raster objects. This ensured that treetops and tree crowns derived from lidar appropriately positioned for spectral extraction of hyperspectral spectra. Each tile was subsequently used to raster model 2000x2000 0.5m raster images using the maximum elevation value from all class 1 and 2 points contained within the cell boundary.

1m Wide Cross Section Profile of Point Cloud Height Distribution and Resulting Maximum Elevation Binning for DSM

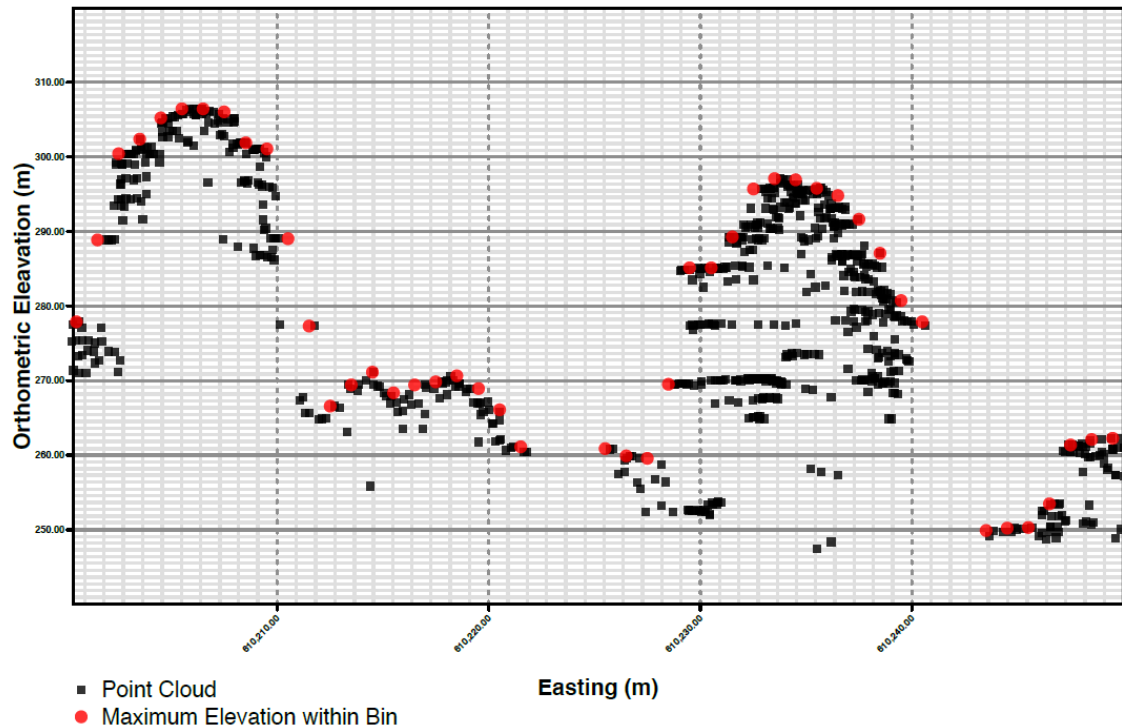


Figure 5. Lidar point cloud cross section and maximum-z DSM gridding representation

This technique was employed as to not interpolate new elevations in the output raster wherever possible preserving the original elevation of the highest returned lidar posting wherever possible. Small data gaps in the output DSM were filled using linear interpolation. Large water features in the project area were characterized by low to non-existent point density and therefore created voids in output raster tiles. To provide a valid elevation for these features, hydro flattening was employed (Heidemann, 2012). Hydro flattening is a procedure where vector representations of the water body were used to create raster masks attributed with the mean elevation of the point returns found within the water body. These water masks were then mosaicked into the raster elevation tiles, therefore creating a continuous valid surface for the rectification procedure.

2.5 INS Trajectory and Integration

Inherent to the design and function of AIS is the requirement of trajectory information that adequately models sensor position and orientation for each sequentially acquired line. In the absence of an accurately synchronized trajectory, raw flightlines consist of a time series of precisely timed sequential scan lines as depicted in Figure 6. If no lines are logged as being dropped it is possible to determine the duration of the flightline accurately by multiplying the number of lines by the inverse of the frame rate. While this duration is accurate, the Start of Line (SOL) event marker may not be accurate due to time lags in the acquisition system. Examining a raw flightline provides a qualitative interpretation as to general platform attitude throughout the survey but without trajectory data, the required External Orientation (EO) of the sensor's perspective centre for each sequential scan line cannot be determined, and scan lines cannot be positioned in a mapping reference frame.



Figure 6. Raw AIS Flightline depicted as a sequential time series

The Applanix POS/AV 410 and 510 were used for the King Island and Pack Lake survey respectively. The POS/AV integrates positional information from the onboard GPS sensors as well as orientation measurements recorded from the IMU; this information is used to model the trajectory. The IMU consists of three pairs of accelerometers and

gyroscopes mounted orthogonally to enable the determination of angular orientation in respect to the three principles axes of the platform. The three axis are typically denoted as, x positive towards the nose of the aircraft, y positive towards the left wing tip, and z positive towards the top of the aircraft (Muller & Lehner, 2002). Roll angle ω , is measured with respect to the x axis, pitch ψ with respect to the y axis, and finally heading angle κ , measured with respect to the z axis.

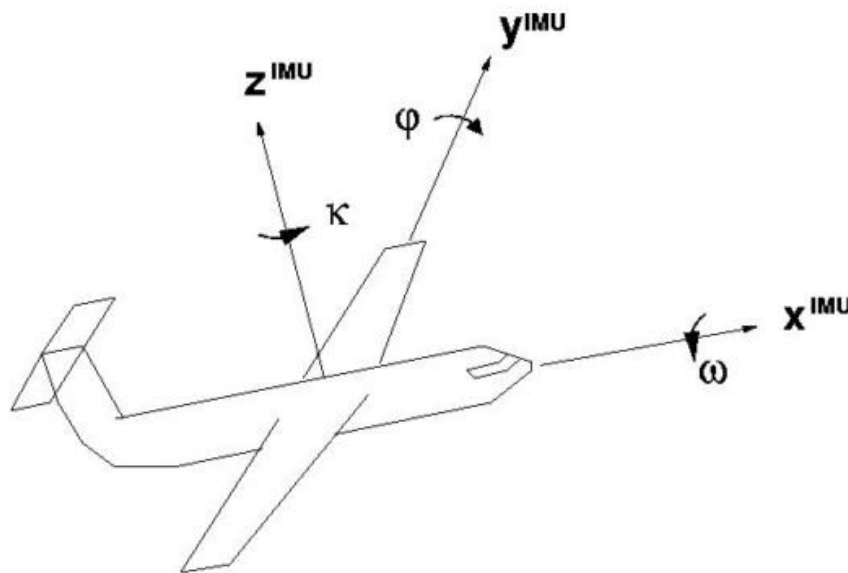


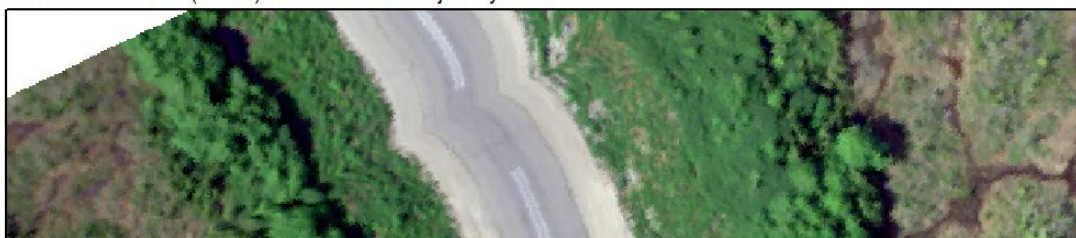
Figure 7. IMU Orientation Reference Frame (reproduced from Muller *et al.* 2002 p.3)

The purpose of a gyroscope is to measure change in angular velocity with respect to each axis, enabling the determination of platform orientation in respect to each axis. The purpose of the accelerometer is to measure the linear acceleration of the platform in respect to each axis. Post processing of the GPS position and IMU orientation through POSPac software provides a Smoothed Best Estimate of Trajectory (SBET). The SBET file contains GPS time stamped records of position and orientation at up to 200Hz; however for the two presented surveys this data was resampled to 50Hz providing a trajectory satisfying the suggestion by Muller & Lehner, (2002) that the INS frequency be at least as high as the AIS frame rate. The EO parameters provided by the SBET trajectory file are referenced to the INS reference point and co-ordinate system origin.

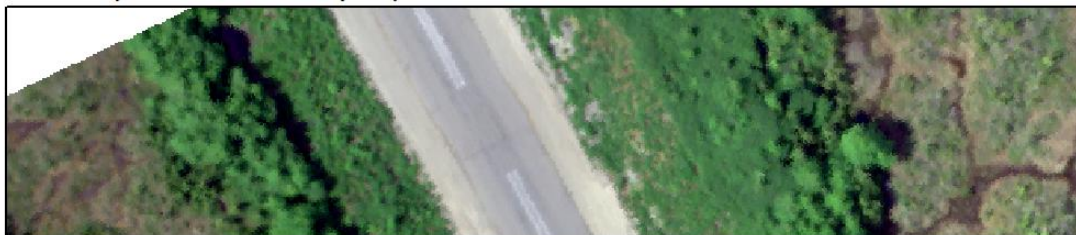
The AIS is slightly offset in position and orientation from the INS reference point, it is therefore necessary to relate the EO parameters to the AIS perspective center through the use of measured offsets called lever arm offsets. To determine the angular misalignment between the INS co-ordinate system and the AIS co-ordinate system it is necessary to calibrate the system using a boresight calibration detailed in Section 2.6.

To utilize the trajectory information in the SBET file for positioning AIS scan lines it is necessary to ensure that the SOL event is accurately synchronized. This synchronization is essential for appropriate attitude data being used to position each scan line using the appropriate exterior orientation. AIS flightlines that are not time synchronized with trajectory information are evidenced by distorted geometry in rectified data. This distortion is particularly apparent when a poorly synchronized flightline has been imaged over a long linear feature, aligned parallel to the along track dimension of the flight, during a high amplitude roll event. The result of this roll event is linear features appearing distorted due to inappropriate attitude data being utilized during the rectification (Figure 8).

SOL Time -1 Frame (-25ms) offset from INS Trajectory Data



SOL Time Synchronized with INS Trajectory Data



SOL Time +1 Frame (+25ms) offset from INS Trajectory Data



Figure 8. Effect of poor time synchronization between INS and AIS

To ensure that time synchronization could be detected and corrected if necessary; all calibration flightlines were imaged with an intentional diagnostic roll feature over linear features as depicted Figure 9.



Figure 9. Synchronized Raw Image with roll attitude plotted in blue line

Flightlines with poor time synchronization were adjusted using an iterative procedure by rectifying flightlines with small time intervals until no distortion was apparent in along track linear features imaged concurrent to roll events. To ensure that appropriate linear features were selected for this process they were selected from concurrently imaged ortho-images and lidar intensity images.

2.6 Boresight Calibration

The boresight calibration procedure for the Aisa Eaglet is similar to other systems that employ direct georeferencing. Direct georeferencing utilizes the exterior (x,y,z) and attitude (roll,pitch,heading) of the sensor combined with the interior orientation of the sensor to derive the exterior orientation of the sensor's across track field of view, and where this intersects with the digital surface model. The major benefit of this system is that no ground control is needed (Muller & Lehner, 2002), other than to validate the calibration and rectification results. The AISA Eaglet is mounted physically close to the

platform Motion Reference Unit (MRU); however slight angular differences exist between the mounting of the MRU and the AIS sensor co-ordinate systems. This misalignment between the sensor co-ordinate systems causes distortions and positional biases to rectified imagery if it is not accounted for through calibration and estimation of misalignment angles.

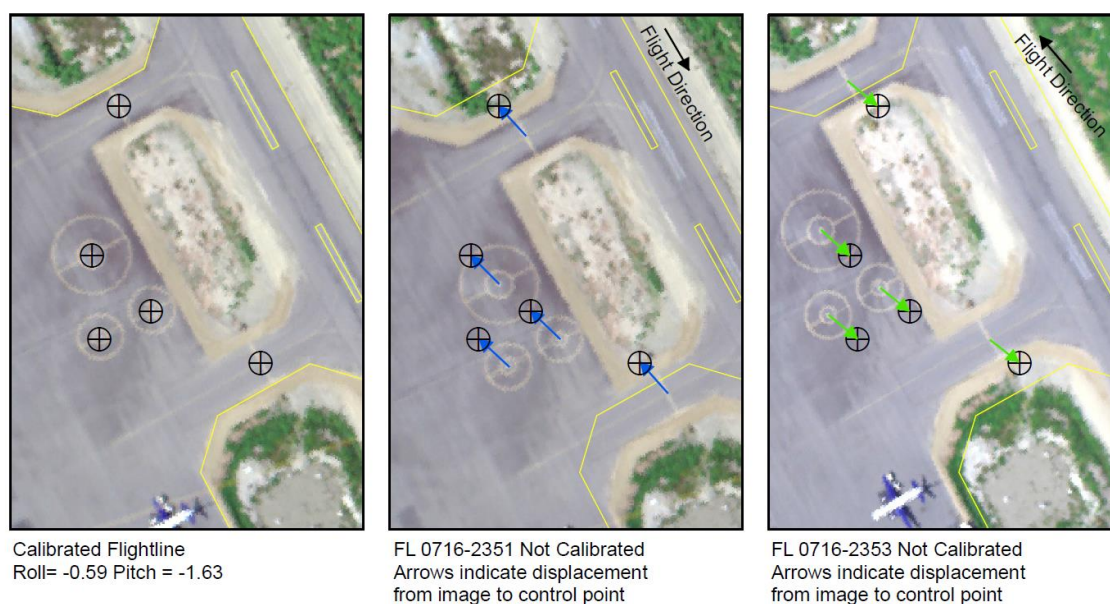


Figure 10. Effect of AIS Boresight Misalignment Angle on uncalibrated flightlines

The inherent angular misalignment between the ALS and IMU's co-ordinate systems can be estimated utilizing a calibration procedure called boresighting. The boresight calibration procedure utilizes flightlines that are imaged over a flat calibration area with a series of flightlines that both overlap and intersect with objects that can be both identified and assessed within the image flightlines (Yastikli, Toth, & Brzezinska, 2008). In the case of the King Island survey, the Bella Bella airport ($52^{\circ} 10' 56''$ N $128^{\circ} 9' 15''$ W) was imaged and surveyed using a calibration pattern. The Bella Bella airport consists of well-defined runway paint lines useful as ground control points, as well as tie points to enable assessment of both relative line to line calibration as well as absolute accuracy.

To validate and assess the boresight calibration, lidar intensity raster images were modeled at 0.5m spatial resolution. Average intensity was calculated for each cell using

all lidar returns in the ground and default classes. The output intensity raster had a radiometric range of 14bits and was used to iteratively assess and adjust roll, pitch, and yaw misalignment angles observed between overlapping linear features from each of the calibration flightlines. Utilizing this iterative procedure enabled a positional accuracy where control points between adjacent lines were found to be coincident within +/- 1 pixel.

2.7 Direct Georeferencing / Orthorectification

The EO parameters refer to the six, position (X_0 , Y_0 , Z_0) and attitude, (roll ω , pitch ϕ , and yaw κ) that define the sensor acquisition geometry at the time of image acquisition. Traditionally photogrammetry using frame cameras has used well defined ground points to, through a process of aerial triangulation, estimate the six EO parameters (Cramer, Stallmann, & Haala, 2000). The estimation of these parameters using ground control points is a form of indirect orientation for georeferencing. Pushbroom AIS systems such as the AISA series sensor do not expose and collected full frame images and instead acquire sequential scan lines through the forward motion of an airborne platform. Each sequential scan line has an associated set of six EO parameters necessary for the georeferencing a scan line. Unlike a frame camera these EO parameters cannot be estimated using an indirect method such as aerial triangulation partially due to the inability to resolve ground locations using a single scan line, and the impractical necessity of needing ground control points for each scan line. Direct georeferencing utilizes the INS to directly measure orientation of the IMU and through the use of lever arm offsets and boresight calibration enables the per scan line EO to be determined directly.

The EO measured through the INS enables the sensor perspective center geometry to be determined for each scan line, but it is the integration of an appropriate elevation model that is important for orthorectification of sensor recorded pixels. Orthorectification is necessary to reconstruct the scene geometry that is recorded using the AIS in a sensor co-ordinate system into a projected co-ordinate system. The orthorectification procedure

ensures that surface features are geometrically correct and where sensor optical distortions are minimized, topographic relief is accounted for and trajectory information including instantaneous platform roll, pitch and heading are utilized for accurate scan line positioning.

Orthorectification of AIS data utilizes the EO parameters to project and, ray trace, a scan line specific sensor to DSM vector determining the intersection with the surface model (Schlapfer & Richter, 2002). The onboard Applanix POS A/V 410 & 510 is capable of high accuracy positioning and orientation at up to 200Hz, exceeding typical frame rates used for the AISA systems that tend to acquire not higher than 100Hz, enabling an optimized dataset for attitude as suggested by (Muller & Lehner, 2002). The limiting data source for determining accurate intersection of AIS data is therefore the elevation model used for orthorectification. The simultaneous survey of nearly coincident discrete multi-return ALS with the two MAP systems enables a high accuracy DSM to be produced with multiple returns for most terrestrial features enabling a top of reflective canopy surface model to be gridded and if necessary modelled over large water features. The lidar system used for the two survey areas typically has a range resolution of 5-10cm, being a fraction of the smallest rectified AIS data and exceeding the guidelines for an elevation models accuracy as set out by Muller & Lehner, (2002).

Chapter 3 – Tree Object Representation, Feature Extraction and Classification

3.1 Introduction

The close integration, calibration and rectification of AIS data through the use of complimentary ALS data and derivatives provide a unique opportunity for further data integration and fusion harnessing OBIA techniques. OBIA provides techniques to segment image data into real world objects taking advantage of context and attribution for analysis. For this forestry based project using OBIA, individual trees are the specific objects of interest for analysis and are segmented through the use of an ALS derived CHM, and field surveyed tree positions. It is important to note that the CHM used for AIS segmentation is a ground normalized version of the DSM used for rectification with aligned pixels between all three data products. This pixel alignment enables structural information derived from the CHM to be used to segment the AIS data without alignment problems or resampling of AIS data; a problem common with projects using separate acquisitions and incompatible ALS geometries as evidenced in (Michael Alonzo, Bookhagen, & Roberts, 2014). The use of OBIA forces an examination of the remote sensing scene models that relate image resolution to the object scale as outlined by (Strahler et al., 1986). Strahler et al. suggested that when the image resolution is high in comparison to the size of the object, an H-resolution model exists, whereas when the resolution is low and the size of the object is smaller than the pixel an L-resolution model exists. With high resolution AIS on the order of 0.5-1.5m resolution as collected by the AISA series in these two projects an h-resolution model prevails for many of the trees in this project enabling segmentation of AIS data using a tree object and within object spectral sampling. Segmentation using tree objects ensures that only pixels coincident with the defined object are extracted for classification reducing the likelihood of spectra being extracted from adjacent land cover types. The concept of image segmentation using tree objects is not new to the remote sensing discipline and has been used in both

automated methods to detect a tree's apex (Wulder et al., 2000), as well as to segment imagery through manual (Mike Alonzo, Roth, & Roberts, 2013; Clark, Roberts, & Clark, 2005) and semi-automated techniques (Jones, Coops, & Sharma, 2010). A unique aspect of this project is the use of ALS used to rectify the AIS, derive tree objects, and finally segment the AIS utilizing the same ALS data.

To accomplish the goal of crown coincident spectral extraction, a tree-based, object model was defined. Individual trees are the primitive object of interest being defined and can be represented simply, by the geographic point or co-ordinate occupied by the tree. This one dimensional point location typically represents the apex of the canopy or geometric center of the crown and is structurally related to the highest vertical extension of the canopy. The crown apex, or treetop can be determined by field survey techniques, through spatial filtering techniques utilizing lidar, or using raster-based local maximum filtering techniques.

The use of individual tree canopies is well established in airborne remote sensing for the detection of tree apex's and canopies. Early work to detect ITC's relied on an observation in optical imagery of the brightest pixel in a local neighborhood was close to or at the apex of a tree. Through the use of a static 3x3 search kernel (Niemann et al., 1998) detected treetops from digital ortho-photos. The use of a static kernel that was too small was noted to cause errors of commission, while too large of a static kernel caused errors of omission; to combat this (Wulder et al., 2000) utilized dynamic search kernels and were able to reduce the error of commission.

The second tree-based object is an object based representation of the crown outline as would be projected on the ground surface. The crown outline is a two dimensional polygon that estimates the unique footprint of the crown outline based predominately on the conical morphology typically displayed by coniferous trees. The two-dimensional object based definition of a treetop and tree crown rely on physical structure and morphology to enable segmentation of the AIS imagery and finally feature extraction based on this structure.

The use of OBIA segments the spectral imagery into an object domain reducing the occurrence of spectral extraction from objects other than the ones of interest. In the case of tree-based extraction, this removes spectral information from open exposed areas, water features, and low vegetation based on the exclusion of objects below a certain height threshold. The ability to extract spectral information on a per crown basis using an object-based method enables spectral evaluation and filtering using within crown spectra and their associated lidar height information.

This chapter describes the use of an object based approach for individual tree representation and subsequent classification using integrated field survey, ALS, and AIS data. An object-based model for this research was chosen based on the need to improve existing forest inventories that are typically estimated at a plot or stand level. The transition from stand, and plot species estimates and towards individual tree-based inventories is inevitable with high resolution remote sensing technologies providing wall to wall coverage becoming ubiquitous in many jurisdictions.

The first section describes the modelling of treetop, and tree crown-objects for use in image segmentation based on, lidar derived, ground normalized CHM in a raster form. The tree objects attempt to represent, at a stem level, resolvable trees from the lidar CHM. The creation of a spatial database for tree objects is important as it allow a unique identifier to be assigned to each tree object enabling much of the geo-processing and classification results to be related back to the original tree objects. The next section describes how tree crowns were delineated from the CHM for use in the Pack Lake study. Integration of field sample data for both King Island and Pack Lake is presented with the final section describing the spectral classification and results.

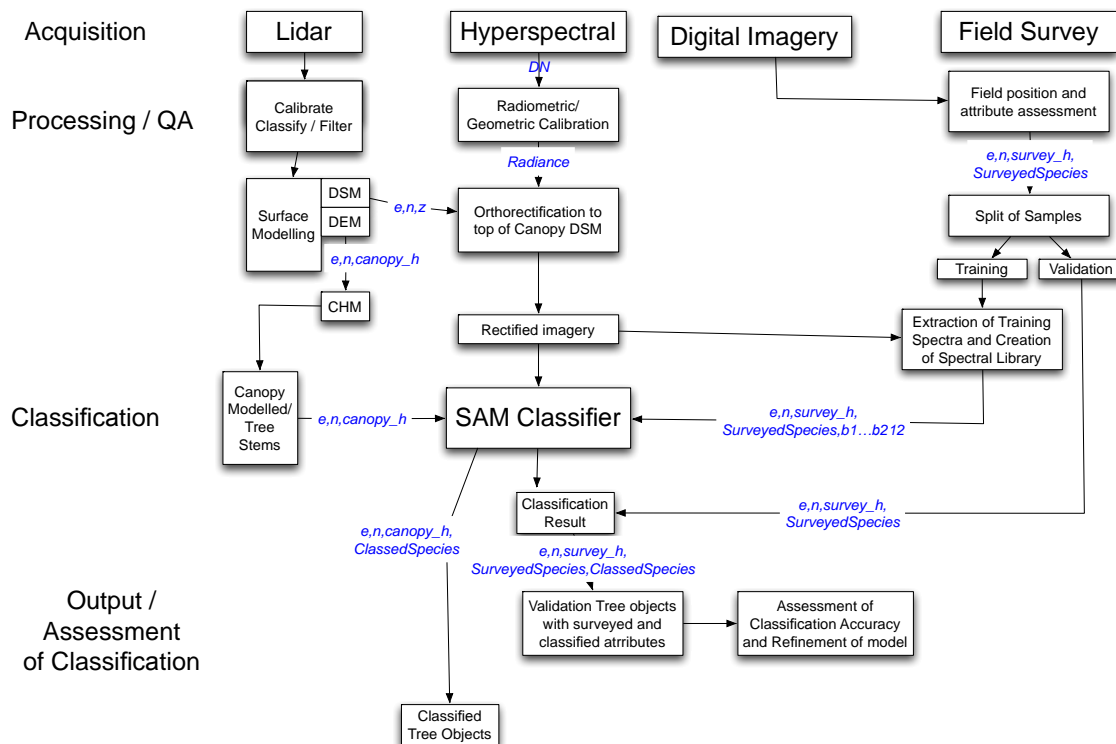


Figure 11. Processing Flowchart

3.2 Point Cloud Normalization

The first step in the treetop detection is the creation of a CHM. The CHM is typically represented as an elevation model in the form of a regularly spaced raster where the elevation values at each cell location represent the highest vegetation height within a cell. In a CHM the ground is the vertical datum and is represented by 0m, each cell height can be compared to others within the study area enabling quick determination of the distribution of heights above ground.

The CHM is enabled through the initial classification of the lidar point cloud into default and ground points encoded as ASPRS LAS file class 1 and 2 respectively. Relatively few returns from the ground surface in dense forested areas necessitated the construction of a TIN modeled surface to represent a continuous surface to which individual default class (1) points could be referenced to. The next step is the normalization of all class 1 and 2 points by subtracting the elevation of the ground as modeled by the tin surface directly

below each point. This normalization process creates a new normalized point cloud in which all ground points have had their initial elevation subtracted from them and now have a height of 0, all default points have been normalized by the ground elevation as determined by the intersection of a point on the tin surface.

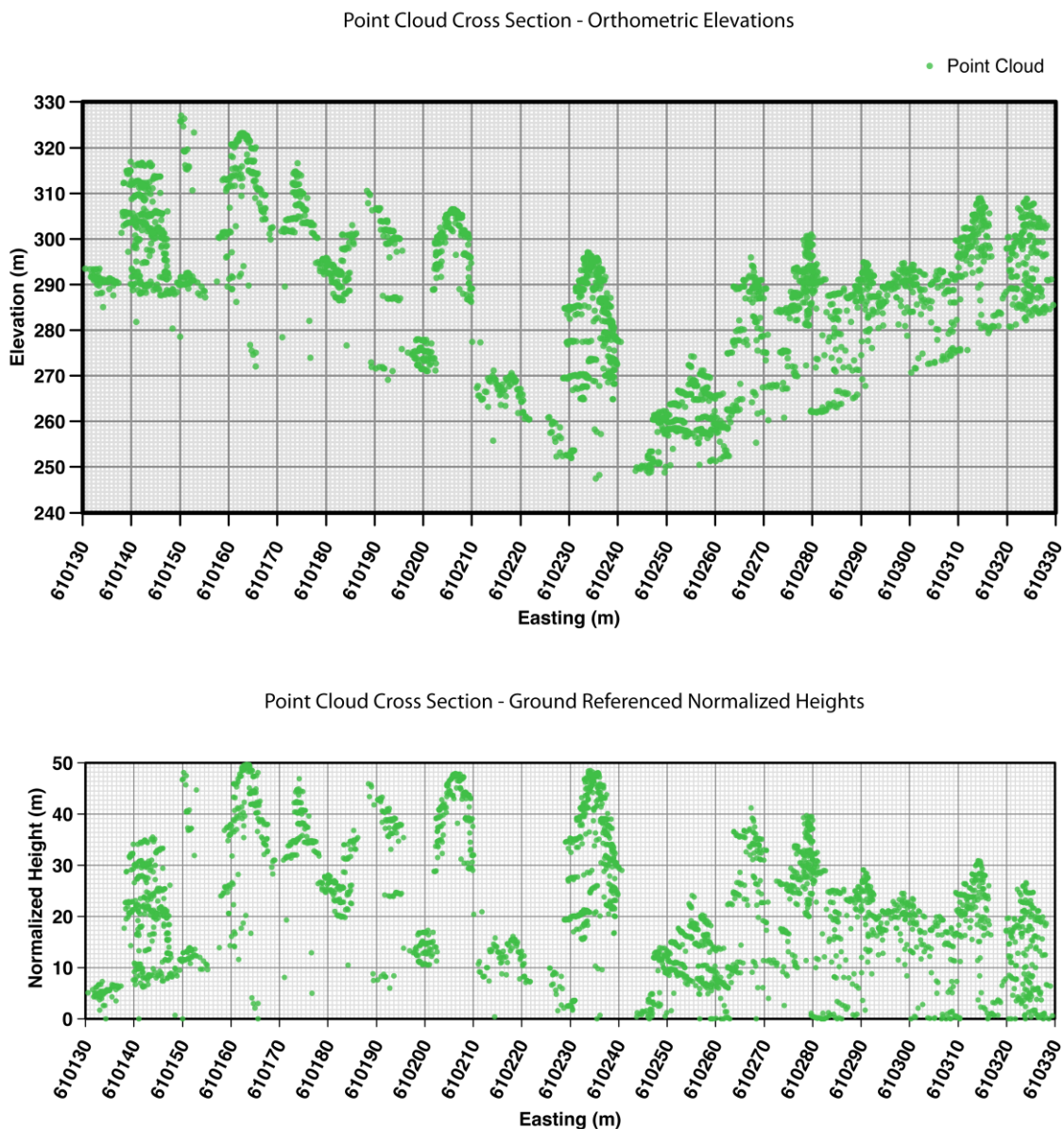


Figure 12. Point Cloud Normalization

3.3 Canopy Height Model Gridding

Modeling a raster based CHM involves gridding the normalized class 1 points. For the two study sites, the output CHM raster was calculated as the maximum height value within a cell rather than the average of all of the point cloud values for that grid cell. Using the average reduces the overall height and does not yield a true measure of the height of the vegetation at that point. Maximum height values are used to enable the use of kernel based raster algorithms for the detection and delineation of individual trees and surrounding canopies.

3.4 Individual Tree Top Detection

The detection of individual trees is enabled through the use of dynamic kernels, defined based on height ranges within the CHM. The concept behind this is that each detectible treetop is represented by a local maximum filter within the raster CHM, where the local neighbourhood is defined by a predetermined kernel of $n \times n$ dimensions centered on the treetop. We noted that the size of the kernel needed to accurately define the tree top varied with the size of the crown. Smaller crowns required a 3x3 kernel size while larger crowns were better suited for larger kernel sizes. As there is an allometric relationship between crown size and tree height, (Avery, 1974), then the determination of the kernel size for a tree of a specified height is based on predefined ranges that increase with greater height values. For the King Island dataset, three ranges were used with three associated search kernels as follows:

Kernel size	Height Range (m)
3x3	3-6
5x5	6-35
7x7	35-100

Table 1. Tree top Search Kernel and Associated Height Range

The 3x3 range is used for tree heights that are between 3 and 6 meters, the somewhat larger trees between 5-35 meters are detected using the 5x5 kernel and larger treetops found using between 35-100 m are found using the 7x7 kernel. This also implies that for the 1m cell size CHM that to satisfy the requirement of being a small treetop, it must be the largest cell within a 3m diameter “crown”, for a medium tree it must be the largest cell within a 5m diameter crown and for large trees it must be the largest within a 7m diameter crown. In this manner, each CHM raster cell that is within the specified ranges has an associated kernel size, however only pixels that are the highest within their height range defined kernel will be considered a treetop. The treetop detection method presented is logically biased towards conifer trees with raster based CHMs that exhibit a local maximum within a height and associated range defined kernel; this has the problem of poor detection of many deciduous trees that do not follow a conical like geometry. For deciduous species this algorithm tends to “detect” multiple false apex’s, within one logical crown leading to errors of commission.

3.5 Individual Tree Crown Delineation

The tree object metaphor was extended for the Pack Lake dataset to enable multiple within crown spectral samples to be extracted. ITCs are defined conceptually based on the footprint of a tree’s crown outline as projected on the ground surface. For isolated trees this outline can be observed in a CHM based on a high magnitude change in height at the edge of the crown and the adjacent surrounding ground terrain. In natural environments the crown outline is more difficult to determine as crowns tend to overlap and intersect with neighbouring trees. Crowns were delineated using an algorithm that utilizes the raster CHM used to determine treetops, the treetops detected, and a set of stopping rules. The algorithm utilized is similar in method to that used by (Tiede, Hochleitner, & Blaschke, 2005). In an OBIA context the tree top is now an object primitive, while the ITC delineated is the real world object (Benz, Hofmann, Willhauck, Lingenfelder, & Heynen, 2004). Crown delineation starts based on the pixel location of the highest treetop; using a local 3x3 kernel each of the surrounding pixels are

determined for membership in a crown object if they meet a defined set of criteria or rules. The rules for crown membership are 1) height being lower than the seed pixel, 2) the height of a candidate pixel being greater than a defined percentage of the CHM and 3) a pixel being within a max crown radius associated with the initial seed point. If each of these criteria is met the pixel is added to the crown and iteratively each added crown evaluates its outward neighbours to determine their membership within the crown. The crown region grows until no crown pixels have neighbours that satisfy membership within the crown object. Pixels delineated using this algorithm are masked once a crown has been defined and are not available for membership in subsequent crowns. For the Pack Lake dataset the following height ranges, and rules were used:

Range (m)	Percentile	Crown Radius (m)
3-35	75	3
35-70	65	6

Table 2. ITC Stopping Rules

The effect of the above ranges was that no CHM pixels were considered if their height was less than 3m, two classes of trees based on heights were delineated with small trees between 3-35m height being used as seed treetop pixels to delineate crowns up to a 3m radius as long as candidate crown pixel heights were at least 75% of the seed treetop value. For larger trees between 35-70m a crown could be delineated up to 6m in radius if a candidate pixel was at least 65% of the seed treetop value.

Similar to the treetop detection, tree crown delineation and segmentation using this simplified model exhibits difficulty in the detection of deciduous canopies. As mentioned above, deciduous trees often have multiple local maxima within the canopy causing multiple treetop representations. These multiple treetops form the seed points for crown delineation and segmentation producing small multiple crowns, “within crowns” in some deciduous trees. Deciduous trees are also problematic as their morphology does not

represent an inverted watershed or cone with the same apex to crown edge slope found with conifers. Shallow slopes and inflections within the slope of the crown cause problems with the percentile based stopping rule with region growing terminating at some inflection points causing small crowns. For coniferous species multiple local maxima and treetops are found within one logical delineated caused by two trees growing in close proximity to each other, candelabra features or tree that has had natural damage affecting the simplified cone geometry required for this algorithm. Multiple treetops are realities within a single crown delineated using these stopping rules but have yet to be managed from a data processing perspective for future segmentation. Finally, it needs to be pointed out that for both the tree detection and the crown delineation, a smoothing filter is required to be run to on the raster CHM to reduce noise and to reduce the likelihood of multiple treetops found within a local kernel. While a smoothed CHM is used for detection and delineation, the position and height of the local maximum is always extracted from the original CHM dataset.

3.6 Spectral Extraction

The classification of tree species for the two study areas required the integration of field based data representing tree species of interest to create objects for image segmentation and feature extraction. The two study sites, King Island, and Pack Lake were analyzed sequentially and progress conceptually from the use of a one-dimensional object for tree extraction for King Island to a two-dimensional crown based object for the Pack Lake dataset. The following sections outline the collection, and evaluation of field data, spectral extraction and finally classification and evaluation of spectra.

3.6.1 Field Survey Data – Collection and Assessment

Field data representing plots and stems of leading species for both the King Island, and Pack Lake study were provided by Strategic Forest Resource Management Inc. The datasets provided consisted of plot locations surveyed in the field using a Trimble GeoXT

mapping grade GPS in conjunction with tree stem locations, associated mensuration and attribute data.

Field surveys of stem locations are essential to train and validate classification algorithms as used in image analysis but must be assessed in terms of position and attribute integrity. GPS positional accuracy may not be good enough in steep sloped, dense forest areas due to poor satellite coverage and a high multipath environment. The number and position of GPS Space Vehicles (SV) available for a positional fix can be occluded based on steep terrain that masks and occludes the SV transmitted radio signal, the result of this can be a sub-optimal constellation for GPS positioning and degradation in differentially corrected position. Dense forest areas characterized by the study sites present a secondary challenge in terms multipath, of radio signals transmitted by SV's interacting with reflective objects existing in the path between the SV and the GPS instrument. This condition causes a delay in the reception of signal due to a longer path length contributing to spurious range calculations and a poor positional solution. Field surveyed stems in this study were positioned using an azimuth and distance offset from the plot centered point surveyed by the GPS; as such these positions are intrinsically biased by poor GPS positions of the plot centre. Positioning of stems is typically represented by the edge of the tree at Diameter at Breast Height (DBH), offset to the centre of the trunk by half the DBH value or radius. While the center of the trunk as referenced by an offset provides a logical geometric centre for stem positioning it can be a poor match for spectra extracted using remotely sensed imagery where a treetop or crown apex pixel may provide optimal illumination, albedo, and potentially signal. This problem is best evidenced in trees where the apex and trunk centre are not horizontally coincident due to leaning or natural growth pattern. Field samples where the comment attribute contained information suggesting leaning were removed from the stem database to mitigate against obviously offset ground to apex positions.

Previous passive optical studies have indicated a potential benefit for the use of crown apex pixels based on high signal and low spectral variation. Based on this research it was thought that spectra located close to the apex would provide the best quality spectra for

classification purposes based on optimal signal and by capitalizing on a simple one-dimensional extraction location thought less likely to be influenced by neighbouring trees of other species where a multi pixel per crown approach may extract spectra from a neighbour.

3.6.2 Training Database Spectral Extraction – King Island

The King Island study site utilized the field surveyed positions of tree species provided by Strategic Forest Resource Management (SFRM) to construct a spectral endmember library based on the spectral responses as extracted from positions of species as field surveyed. While 503 field surveyed stems were provided, 495 were coincident with hyperspectral flightlines and available for spectral extraction, classification and validation of species of interest.

Tree Species	Class Code	n
Amabilis Fir (<i>Abies amabilis</i>)	Ba	18
Western red cedar (<i>Thuja plicata</i>)	Cw	342
Western hemlock (<i>Tsuga heterophylla</i>)	Hw	103
Sitka spruce (<i>Picea sitchensis</i>)	Ss	20
Yellow Cedar (<i>Chamaecyparis nootkatensis</i>)	Yc	12
Total		495

Table 3. King Island Field Surveyed Stems Training Data Distribution

For each field surveyed position in the King Island training database a coincident hyperspectral signature was extracted. During this stage of the research project it was felt that a single spectrum positioned at the highest point of the tree would be optimal in terms of albedo and spatial confidence within the crown. Each candidate field position was assessed in terms of encoded attribute information including species code, cruise

height, spatial confidence and field report comments. These database attributes were assessed in conjunction with orthophotos, raster canopy height model, and point cloud in terms of positional information and attribute integrity. Any samples that had obvious integrity issues were removed from analysis.

Each extracted spectrum was encoded using a unique identification attribute that linked the spectra back to the field surveyed stem database. The unique identifier attribute consisted of the species code followed by a serial number unique to the stem. The wide field of view of the AISA Eaglet combined with areas of high relief caused occluded pixels, under sampling and high off nadir acquisition geometries. To maximize for spectral extraction of features close to nadir geometry, each sample was assigned to the nearest flightline. For each flightline the assigned features were extracted and encoded by unique identifier and species code. On a per species basis, descriptive statistics were calculated to visually assess and interpret spectral signatures on the basis of their mean, standard deviation and co-efficient of variance. In addition the mean calculated spectra for each species class was used for exploratory classification and to provide a means to compare the multi-endmember approach.

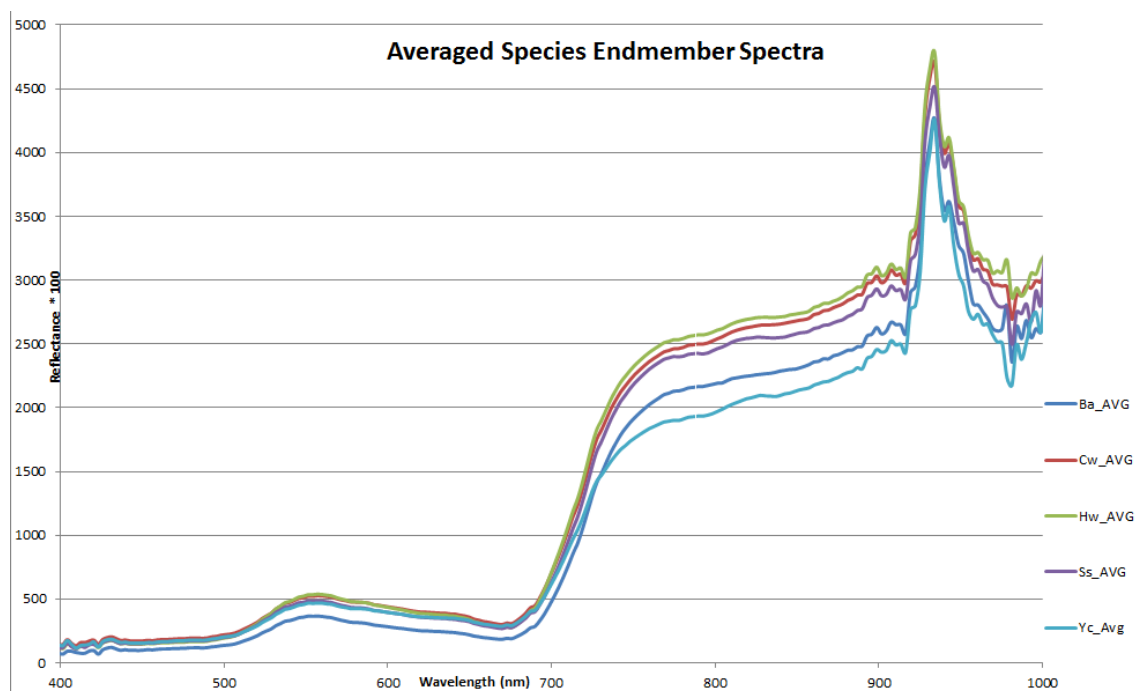


Figure 13. Species Average Reflectance

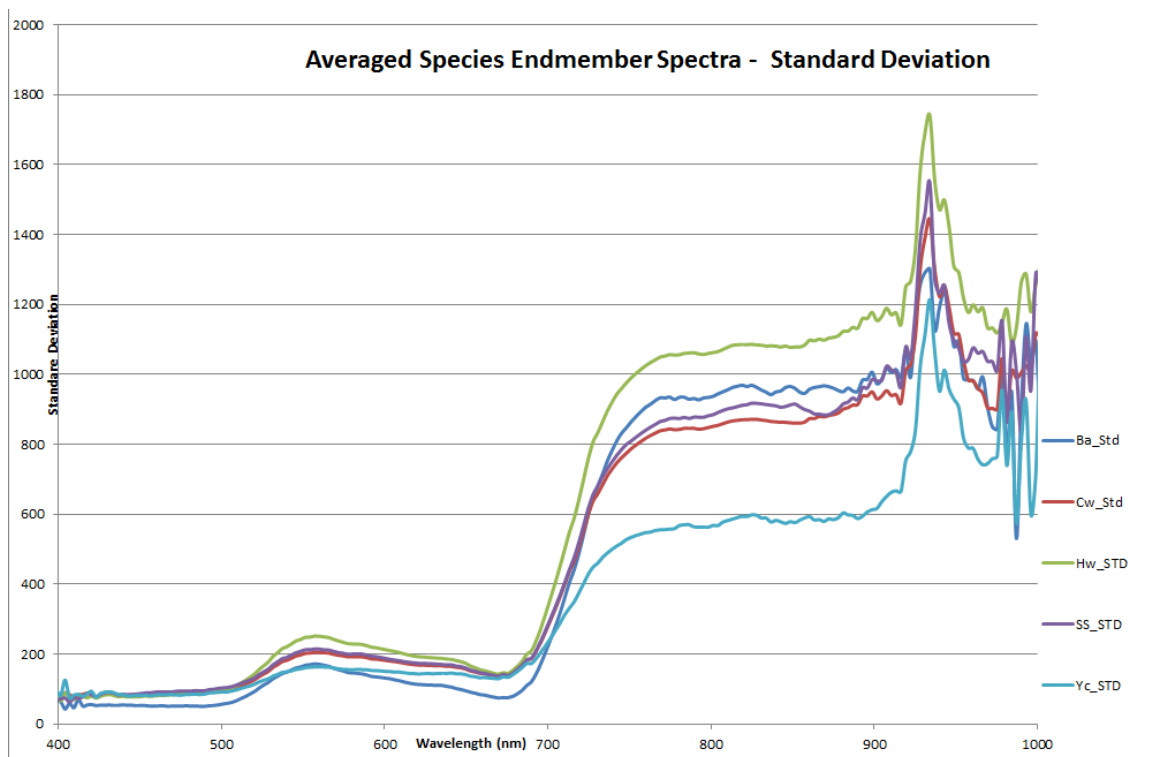


Figure 14. Averaged Species Standard Deviation

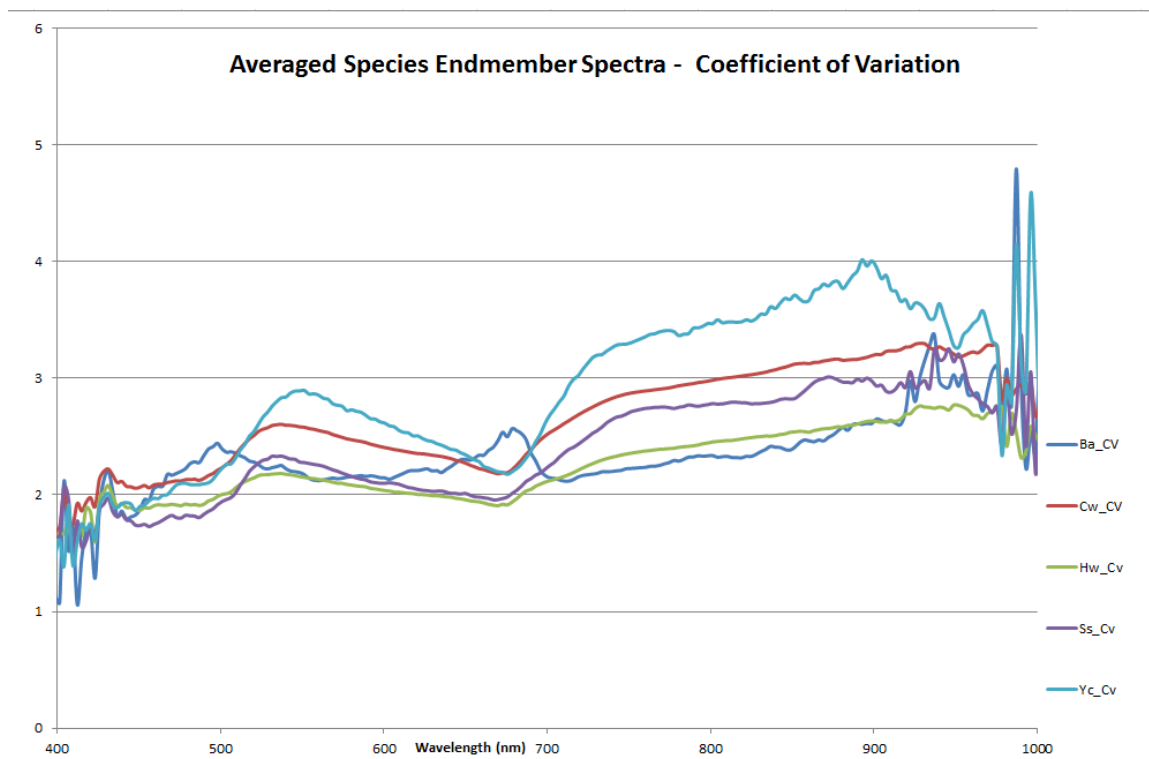


Figure 15. Averaged Species Spectra- Coefficient of Variation

3.6.3 Training Database Spectral Extraction – Pack Lake

The Pack Lake study consisted of a similar coastal site to King Island and benefited from advances occurring with ALS/AIS integration and fusion being researched at the Hyperspectral and Lidar Research Group (HLRG). In contrast to the poorly balanced King Island field data, the field sampling for the Pack Lake study site was more equitably distributed for dominant species including collection of Red alder, a deciduous species.

Further refinement of ITC based detection and delineation provided an opportunity to examine the extraction of field positioned tree spectra utilizing a two-dimensional canopy object segmented from the lidar. The distribution of species surveyed for Pack Lake is presented in Table 4, and depicts the number of candidate field samples available for ITC extraction; the low sample size of Mountain hemlock necessitated its removal from analysis.

Tree Species	Class Code	n
Amabilis Fir (<i>Abies amabilis</i>)	Ba	33
Western red cedar (<i>Thuja plicata</i>)	Cw	65
Red Alder (<i>Alnus rubra</i>)	Dr	33
Mountain hemlock (<i>Tsuga mertensiana</i>)	Hm	2
Western hemlock (<i>Tsuga heterophylla</i>)	Hw	66
Lodgepole pine (<i>Pinus contorta</i>)	Pl	21
Sitka spruce (<i>Picea sitchensis</i>)	Ss	17
Yellow cedar (<i>Chamaecyparis nootkatensis</i>)	Cy	33
Total		270

Table 4. Pack Lake Training Species Distribution

The first step in integrating the field based stem for tree crown spectral extraction involved geoprocessing of the field data provided for the study area. Field samples of

species of interest were provided as a shapefile intended to represent the treetop of candidate trees. For each database record, species, tree height, and other attribute information was presented. The ITC vectors that were delineated from lidar provided a systematic approach to delineating crowns using segmentation stopping rules based on height, percentile and radius that were applied evenly to each raster cell in an image. This methodology removes some of the arbitrary decisions that could be introduced from a human interpreter. At the outset of the project, part of the field data integration and geoprocessing involved the plan to use ITC vectors for the spatial joining of field surveyed tree objects, effectively promoting the point attribute to the enclosing ITC polygon. An aspect not perceived about the Pack Lake field survey data was the existence of field survey positions where two trees were closely clumped together, occurring for both same and differing species. The result of clumped field surveyed trees is that some ITC polygons from the lidar would contain multiple-species class features creating an ITC object with ambiguity towards its species designation. To ensure a logical one to one relationship between ITC and field surveyed points, all ITC polygons that contained more than one field stem were not permitted in the spatial join. The remaining ITC polygons were now featuring aware of the field surveyed trees they encompassed.

The use of an ITC object model was implemented in such a manner that it was used both as a structure based segmentation object as well as unique tree object within a geographic database that was attributed from multiple data sources. A custom designed software tool was used to subset the ITC polygons attributed with field data, extract coincident CHM heights, lidar point cloud, and AISA Eagle rectified reflectance within the crown boundary. In opposition to the one flightline pixel per tree object used for the King Island project, the Pack Lake dataset increased the spectral sampling of crown object where they intersected multiple flightlines. Part of the ITC driven extraction involves the calculation of crown specific lidar and spectral metrics including location albedo and crown relative albedo.

To explore effect of albedo for classification, ITC spectra were extracted based on a filter where the top 50% albedo pixels were extracted for use as ITC endmembers to use for

extraction and classification. The input into the Pack Lake Spectral Angle Mapper (SAM) classification were an endmember library consisting of spectra attributed with the parent ITC, crownID, unique field survey stem ID, and species code. Additional attributes could be examined by using a database table join if necessary.

3.7 Classification

ITC based spectra extracted using the one-dimensional ITC model introduced for the King Island Project and the two-dimensional ITC model for Pack Lake were both implemented using the SAM classification scheme. The following sections detail the classification performed for the two study sites.

3.7.1 Spectral Angle Mapper

The classification of extracted tree spectra was based on a modification of the non-parametric SAM described in (Kruse et al., 1993). The SAM algorithm enables an angular calculation of spectral similarity between a known spectra and unknown spectra. The angle is calculated between a pair of n-dimensional vectors representing the two target spectra. Low spectral angles indicate spectral similarity, while high values are indicative of spectra with differing shapes. SAM is theoretically insensitive to changes in albedo as it is the relative angle between unknown and known spectra not the length of the vector representing the spectra of interest that is calculated.

$$\cos^{-1} \left(\frac{\sum_{i=1}^n t_i r_i}{(\sum_{i=1}^n t_i^2)^{1/2} (\sum_{i=1}^n r_i^2)^{1/2}} \right)$$

Equation 3. Spectral Angle Equation

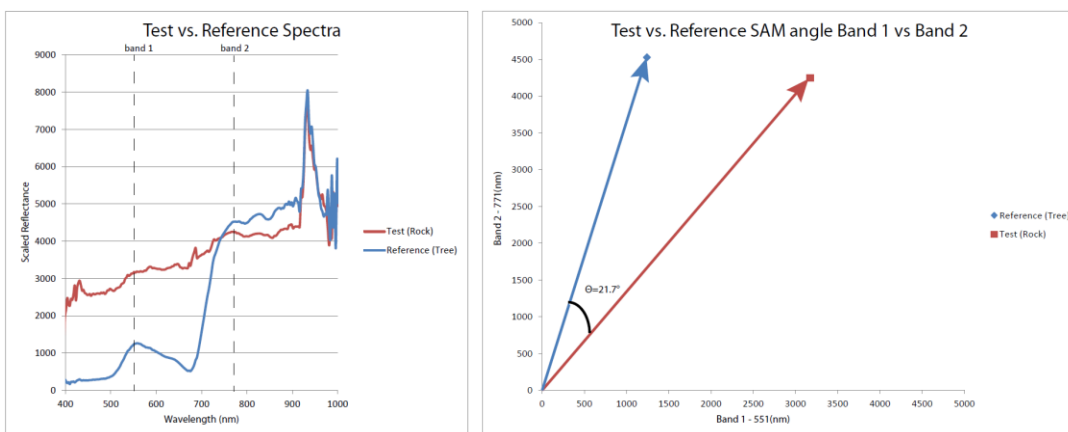


Figure 16. Spectral Angle Example

To create reference spectra, field surveyed stem locations were used to guide extraction using two techniques both utilizing a multi-endmember approach. The multi-endmember approach attempts to characterize the inherent natural variability that occurs with intraspecies reflectance spectra due to bio-chemical and bio-physical differences (Bateson, Asner, & Wessman, 2000; Debba, Cho, & Mathieu, 2009). For the King Island study, multiple endmembers per species class were extracted utilizing field surveyed positions to guide top of reflective canopy spectra. For the Pack Lake study, field surveyed locations of stems were used as seed points to guide a crown object-based segmentation, multiple endmember spectral extraction and classification.

3.7.2 Individual Tree stem based classification – King Island

The SAM algorithm was used for two approaches for the King Island dataset. The first method utilized the average spectra on a per species basis to examine the performance of per species mean spectra for classifying all members within the database. For the average spectra method each endmember in the database has an angle calculated between it and each species averaged spectra. The lowest calculated angle between test and average spectra indicates the best match of spectral similarity. To assess how well mean spectra are capable of classifying spectra of their own nominal species class, a classification matrix is used to enumerate the number of times the test spectra were classified closest to

each average endmember. Through the use of a confusion matrix performance of the classifier can be assessed.

The second method is based on the cross validation leave one out method and is often applied where low samples do not provide adequate data for training and validation. In this SAM classification method all endmembers become library spectra except for one test endmember, which is removed from the library, having its spectral angle calculated against each library endmember. The closest match, based on lowest angle, and library endmember species code, is recorded for each test spectra enabling a confusion matrix to be tabulated to assess classification accuracy and performance.

3.7.3 Crown Based spectral classification – Pack Lake

The classification for the Pack Lake study area utilized the SAM algorithm using a leave one out cross validation approach to enable evaluation of ITC extracted crown spectra. Using an iterative approach, each crown spectra was removed from the library and the spectral angle was calculated against all members remaining in the library, with the lowest spectral angle, associated spectral ID and species designation recorded. Tabulation of smallest spectral angle and class membership per species is presented in the results section.

3.8 Results

The results of the extracted and classified tree spectra are predominately presented through the use of classification or confusion matrices for each of the two study sites.

3.8.1 King Island Individual Tree based SAM Classification Results

The results of the per species average spectra SAM classification for King Island are presented in Table 5.

	Ba	Cw	Hw	Ss	Yc	Row Total	Producers Accuracy %	Error of Omission %
Ba	11	0	2	3	2	18	61.11	38.89
Cw	63	84	78	61	56	342	24.56	75.44
Hw	22	7	47	8	19	103	45.63	54.37
Ss	7	3	5	4	1	20	20.00	80.00
Yc	1	1	2	0	8	12	66.67	33.33
Column Total	104	95	134	76	86	495		
User's Accuracy %	10.58	88.42	35.07	5.26	9.30			
Error of Commision %	89.42	11.58	64.93	94.74	90.70		Overall Accuracy %	31.11

Table 5. Species Average Spectra SAM Confusion Matrix

The confusion matrix presented for the average species class SAM indicate the ability for a set of species designated spectra to be classified correctly through the use of a species class representative average spectral endmember. For each species code the proportion of correctly classified test spectra to the total number of spectra in that species class is indicated by the producer's accuracy. The producers accuracy only considers how well the within class test spectra were able to be classified correctly, the test spectra incorrectly classified as other classes is indicated by the error of omission. In the case of using an average representative endmember spectra, Balsam (Ba) and Yellow Cedar (Yc) both performed better than the other species but were unable to be classified correctly 39% and 33% of the time correctly. For all other species the use of an averaged spectrum produced very poor results. The user's accuracy is a measure of the proportion of spectra that were originally belonging within a class to the number of test spectra actually classified as a species. A low user's accuracy for a class such as Ba is an indication that a very low proportion of spectra classified as Ba were actually Ba. The low user's accuracy for Ba, Hw, Ss, and Yc all indicate confusion between other species and these classes. The relatively high user's accuracy for Cw suggests that despite poor producer's accuracy

and high levels of omission, very few other spectra were misclassified as Cw. The overall accuracy indicates the overall proportion of correctly classified spectra to the total number of spectra.

The second SAM classification technique utilized a cross-validation leave one out approach. The results for the classification in terms of a confusion matrix are presented in table

	Ba	Cw	Hw	Ss	Yc	Row Total	Producers Accuracy %	Error of Omission %
Ba	12	4	2	0	0	18	66.67	33.33
Cw	6	249	65	20	2	342	72.81	27.19
Hw	4	57	33	6	3	103	32.04	67.96
Ss	1	13	4	2	0	20	10.00	90.00
Yc	0	9	2	0	1	12	8.33	91.67
Column Total	23	332	106	28	6	495		
User's Accuracy %	52.17	75.00	31.13	7.14	16.67			
Error of Commision %	47.83	25.00	68.87	92.86	83.33		Overall Accuracy %	60.00

Table 6. Full Range Multi-Endmember SAM Confusion Matrix

The results presented in Table 6 depict a considerable improvement in overall accuracy with large increases to most species for their producer's accuracy. The Balsam producer's accuracy increased marginally, however this is taken in the context of a much improved Ba user's accuracy indicating less confusion with other species being misclassified as Ba. Western red cedar showed a nearly threefold increase in producer's accuracy with associated high user accuracy. Western hemlock had a small decrease in both producers and users accuracy; however that had been spread out more evenly between other species shifting more towards Western red cedar. Sitka spruce had a 50% drop in producer's

accuracy with increased confusion with Western red cedar and less with Balsam. The Yellow cedar class producer accuracy dropped considerably with associated extremely high errors of both omission and commission.

The third classification for the King Island Dataset utilized a subsetted spectral range to try to remove portions of shortwave and near infrared where noise appeared to be evidenced. A spectral subset between 480-850nm utilized an otherwise identical leave one out cross validation SAM as explained for the full range classification.

	Ba	Cw	Hw	Ss	Yc	Row Total	Producers Accuracy %	Error of Omission %
Ba	12	6	0	0	0	18	66.67	33.33
Cw	6	278	47	7	4	342	81.29	18.71
Hw	2	62	33	5	1	103	32.04	67.96
Ss	0	12	4	4	0	20	20.00	80.00
Yc	0	11	1	0	0	12	0.00	100.00
Column Total	20	369	85	16	5	495		
User's Accuracy %	60.00	75.34	38.82	25.00	0.00			
Error of Commission %	40.00	24.66	61.18	75.00	100.00		Overall Accuracy %	66.06

Table 7. Spectral Subset Multi-Endmember SAM Confusion Matrix

The spectrally subset results for King Island show an increase in overall accuracy from the full band multi-endmember and have an associated increase in producers accuracy for all species except for Yellow cedar. The Yellow cedar training dataset was unable to correctly classify any other Yellow cedar, 4 of 5 trees classified as Yellow cedar were in fact Red Cedar. The producer's accuracy also improved for all species other than Yellow Cedar with an associated drop in the error of commission.

3.8.2 Pack Lake Crown based SAM Results

	Cw/Yc	Hw/Ba	Ss	Dr	Pl	Row Total	Producers Accuracy %	Error of Omission %
Cw/Yc	378	101	20	4	34	537	70.39	29.61
Hw/Ba	115	671	34	52	4	876	76.60	23.40
Ss	19	28	52	4	0	103	50.49	49.51
Dr	5	57	3	85	0	150	56.67	43.33
Pl	40	6	0	0	16	62	25.81	74.19
Column Total	557	863	109	145	54	1728		
User's Accuracy %	67.86	77.75	47.71	58.62	29.63			
Error of Commission %	32.14	22.25	52.29	41.38	70.37		Overall Accuracy %	69.56

Table 8. Pack Lake SAM Confusion Matrix

The Pack Lake confusion matrix represents the results of extracting multiple ITC spectra while using albedo thresholding for extracted pixels to maximize the high reflectance pixels with a high signal to noise ratio. Based on difficulty to separating Western Hemlock and Balsam and Western red cedar and Yellow cedar, two aggregate classes were created. The overall performance of the multi-endmember per ITC has a similar overall accuracy to the King Island full range classification and spectrally subset classification but should not be directly compared due to the difference in species classes and aggregated classes. The producer and user's accuracy for Cw/Yc and Hw/Ba depicts reasonable success at Cw/Yc and Hw/Ba test spectra matching with other endmember library spectra of the same classes. Sitka Spruce based on producer's accuracy performs better than the King Island Ss class but still has confusion other coniferous species. Additionally Ss has a high error of commission indicating 53% of spectra classed as

Sitka, are not Sitka Spruce spectra. Red alder has a high degree of confusion with Hw/Ba indicating poor separability between these classes. Lodgepole pine, P1 performs the worst with nearly three quarters of all P1 test spectra classifying as something other than Lodgepole pine.

Chapter 4 – Discussion and Future Work

The assessment of multisensor data integration for ITC based spectral classification has provided a unique opportunity to investigate the effects of acquisition, calibration, georeferencing, and lidar guided segmentation. The relationship between image resolution and object scale are highlighted in the AIS/ALS survey over the King Island project area. At a scene object level, an ITC has a continuous representation ranging from a seedling to old growth trees, creating a dynamic scale relationship between a given sensor resolution and the tree object. For very small tree crowns an L-resolution relationship exists with the AIS data, suggesting a much different spectral contribution from the objects that exist within the IFOV of a sensor pixel. This relationship dynamically changes with tree crowns to a multi AIS pixel per crown relationship, and more of an H-resolution scene object model. For ITC spectral extraction, using a lidar driven structural segmentation, it would be beneficial to determine crown size thresholds where positional uncertainty is assessed for appropriateness for a crown extraction.

Complicating the relationship between a dynamically changing ITC scene object throughout the scene is the dynamic spatial resolution of an ALS, especially when acquired from a rotary platform over a scene like King Island. The constantly changing acquisition geometry to accommodate for terrain and surficial relief, coupled with differing over ground velocities produce a range of across track and along track pixel dimensions. Changes in sensor orientation produce over and under sampled portions of flightlines creating uneven coverage for flightlines and features within them. The use of a nominal square pixel size to represent the combination of flight altitude, and speed over ground/frame rate is always a compromise. If too large of a rectification pixel size is chosen it will imply to the end user that the signal has been acquired spatially over a larger area than the original acquisition condition represents. Conversely the use of too small of a pixel size for rectification will cause many portions of the output rectified data to have null values and at the same time implying less area sampled on the ground. The existence of null values in imagery data causes difficulty for assessment and

interpretation of scene objects and problems for calibration and assessment. These AIS scene resolution and tree object, dynamic scale relationships are compounded by similar scale and resolution problems encountered by the lidar data used for segmentation. A simple scene resolution to object scale mismatch is also encountered through the use of field survey data collected for ITC spectral endmember extraction. If a single pixel coincident with the survey co-ordinate is extracted for classification and training there is an inherent positional uncertainty that is more problematic for within crown object sampling of small crown diameter trees. ALS has similar scene object scale and resolution implications for feature representation and segmentation. If differing resolutions exist between multiple airborne sensors, feature extraction can be influenced by misaligned pixel to pixel alignment, or the vector clipping geometry used to extract raster data. All of these object scale, and resolution relationships influence the spectral information extracted and the representation of the object of interest and should be carefully considered when integrating multi-sensor data.

The classification results do not lead to any direct conclusions regarding the ability to classify individual tree species at an ITC level due to poorly balanced datasets. The King Island dataset had a comparatively large sample size of Western red cedar but the low sample numbers for and representation of species such as, Sitka spruce, Balsam and Yellow cedar do not provide the capacity to draw conclusions on either how representative the extracted spectra are of the indicated species, or if classification accuracy may improve, if a larger sample was available. Western hemlock was a problematic species, particularly with the King Island dataset, as many of the field cruise surveyed stems were attributed with a “cruise height” attribute that indicated that they were either co-dominant trees or suppressed below the dominant leading species. For most of King Island, Western red cedar appeared to be dominant. The problem with the hemlocks that are below the top of the reflective canopy surface is that they tend to be occluded by many sensor acquisition geometries, providing very little in the way of reflectance data that can be ascertained as being completely occupied by the suppressed stem. It is possible that the social position of Western hemlock in relationship to other species caused spectra from the correct planner field co-ordinate to be extracted, yet was

actually was more representative of the species occluding the understory hemlock causing poor classification results. The overall poor performance of SAM based on mean spectra is consistent with previous research by Cho et al (2010) into the use of species specific endmembers represented by a mean or representative spectra. A similar study using mean spectra (Debba et al., 2009) found similar poor classification performance using a similar SAM technique. The increased performance of the King Island multi-endmember per species classification is consistent with other individual ITC research. The slight improvement in performance based on spectral range could be due to noisy spectral regions, but could also be related to research advocating for an optimal band selection method.

The King Island dataset has interesting potential for further classification work through the use of ITC segmentation and spectral extraction. With an increased sample size using crown object for segmentation a more balanced within crown sample for each species could be examined.

The Pack Lake dataset provided a better sample distribution on a per species basis, however was countered by a coarser scene resolution with almost twice as coarse spatial resolution when compared to King Island. This coarser image resolution impacted spatial confidence when using a segmentation driven approach, especially for small crown diameter species such as balsam and pine. The addition of deciduous Red alder to the Pack Lake study proved to be difficult for species classification based on the observed poor classification performance. The poor alder classification could be related to the algorithm used for ITC delineation and the expected conifer object geometry the algorithm performs best with. ITC crown outlines delineated for observed stands of Red alder encompassed a fractional amount of the canopy, likely a result of stopping rules that are evaluated with conifers in the study area. The performance of the classifier was also observed spatially within the context of the scene and suffered from particularly poor performance for trees that were located in the southern portion of the image with a north aspect. This classification performance problem could be related to poor solar illumination geometry and low absolute albedo. Similar to the suppressed Western

hemlocks found in the King Island site, there may have been endmembers included in the library that had very poor signal to noise based on shadowed or partially included geometry. To manage this low albedo, an absolute threshold could be used to remove a training endmember from analysis. This albedo problem would be insensitive to the relative per albedo thresholding that is part of the crown extraction, a low absolute albedo sample that is the highest in a crown will still be extracted.

While the use of OBIA and an ITC segmentation model for AIS canopy classification is not unique to this study, and has been implemented with promising results in both tropical (Féret & Asner, 2013), and urban tree studies (Michael Alonzo et al., 2014), the results can't be directly compared. While the urban and tropical ITC studies referenced above follow a similar methodology for segmentation, and classification, to the two study sites in this thesis, there are many differences that may explain differences in apparent classification capability.

The two mid-coast study sites presented in this thesis are dominated by coniferous ITCs, with the dominant, most abundant, and largest crown size belonging to mature Western red cedars. Other conifers sampled within the study site including Yellow cedar, Sitka spruce, Western & Mountain hemlock, and Lodgepole pine were used for classification purposes; however these ITCs tended to have considerably smaller crown areas, overlapped with neighboring crowns, or were not emergent from the canopy, in the same way that Western red cedar was. In contrast to the two mid-coast studies, the tropical and urban studies cited tend to have rich species diversity, utilize emergent or spatially isolated crowns and have much larger crowns for each of the species studied.

The examination of the end-to-end integration of multi-sensor airborne imaging for an object based classification reveals how interrelated each of the systems is throughout acquisition, calibration, rectification and segmentation. The high level of integration on the MAP series of sensors at a hardware level enables acquisition of ALS suitable for calibration, rectification, and OBIA segmentation for AIS feature extraction. The use of ITC based OBIA using AIS data for coastal forestry applications is complicated by

dynamic acquisition geometry caused by changes in underlying terrain and platform attitude. The use of structure driven lidar based segmentation provides a first step in reducing noise from adjacent scene objects and providing ITC relevant spectra for use in a classification algorithm. It is suggested that future work should continue to examine the within crown spectra extracted, both in terms of their relative albedo and shape, as well as their relationship to other crowns of the same species class. The ITC itself should be examined in terms of overall area, shape, and number of associated AIS pixels to ensure that candidate crowns are appropriate for inclusion with the species class.

Bibliography

- Alonzo, M., Bookhagen, B., & Roberts, D. a. (2014). Urban tree species mapping using hyperspectral and lidar data fusion. *Remote Sensing of Environment*, 148, 70–83. doi:10.1016/j.rse.2014.03.018
- Alonzo, M., Roth, K., & Roberts, D. (2013). Identifying Santa Barbara's urban tree species from AVIRIS imagery using canonical discriminant analysis. *Remote Sensing Letters*, 4(5), 513–521. doi:10.1080/2150704X.2013.764027
- Avery, T. E. (1974). *Natural resources measurements* (2nd ed., p. 71). New York: McGraw-Hill.
- Bateson, C. a., Asner, G. P., & Wessman, C. a. (2000). Endmember bundles: a new approach to incorporating endmember variability into spectral mixture analysis. *IEEE Transactions on Geoscience and Remote Sensing*, 38(2), 1083–1094. doi:10.1109/36.841987
- Benz, U. C., Hofmann, P., Willhauck, G., Lingenfelder, I., & Heynen, M. (2004). Multi-resolution, object-oriented fuzzy analysis of remote sensing data for GIS-ready information. *ISPRS Journal of Photogrammetry and Remote Sensing*, 58(3-4), 239–258. doi:10.1016/j.isprsjprs.2003.10.002
- Cho, M. A., Debba, P., Mathieu, R., Naidoo, L., van Aardt, J., & Asner, G. P. (2010). Improving discrimination of savanna tree species through a multiple-endmember spectral angle mapper approach: Canopy-level analysis. *Geoscience and Remote Sensing, IEEE Transactions on*, 48(11), 4133–4142. Retrieved from http://ieeexplore.ieee.org/xpls/abs_all.jsp?arnumber=5559438
- Clark, M., Roberts, D., & Clark, D. (2005). Hyperspectral discrimination of tropical rain forest tree species at leaf to crown scales. *Remote Sensing of Environment*, 96(3-4), 375–398. doi:10.1016/j.rse.2005.03.009
- Cramer, M., Stallmann, D., & Haala, N. (2000). Direct georeferencing using GPS/inertial exterior orientations for photogrammetric applications. ... *Archives of Photogrammetry ...*, XXXIII(1999). Retrieved from http://www.researchgate.net/publication/250654324_DIRECT_GEOREFERENCING_USING_GPSINERTIAL_EXTERIOR_ORIENTATIONS_FOR_PHOTGRAMMETRIC_APPLICATIONS/file/3deec5283246eb307b.pdf
- Davis, C., Bowles, J., Leathers, R., Korwan, D., Downes, T. V., Snyder, W., ... Risse, R. A. (2002). Ocean PHILLS hyperspectral imager: design, characterization, and calibration. *Optics Express*, 10(4), 210–221. doi:10.1364/OE.10.000210

- Debba, P., Cho, M. A., & Mathieu, R. (2009). *Within- and between-class variability of spectrally similar tree species. IEEE International Geoscience and Remote Sensing Symposium IGARSS 2009* (Vol. 4, pp. IV-272-IV-275). IEEE.
doi:10.1109/IGARSS.2009.5417319
- Féret, J., & Asner, G. (2013). Tree species discrimination in tropical forests using airborne imaging spectroscopy. ... *and Remote Sensing, IEEE Transactions on*, 51(1), 73-84. Retrieved from
http://ieeexplore.ieee.org/xpls/abs_all.jsp?arnumber=6241414
- Heidemann, H. K. (2012). Lidar Base Specification Version 1 . 0. In *Book 11*. U.S. Geological Survey.
- Jones, T. G., Coops, N. C., & Sharma, T. (2010). Assessing the utility of airborne hyperspectral and LiDAR data for species distribution mapping in the coastal Pacific Northwest, Canada. *Remote Sensing of Environment*, 114(12), 2841-2852.
doi:10.1016/j.rse.2010.07.002
- Kruse, F. A., Lefkoff, A. B., Boardman, J. W., Heidebrecht, K. B., Shapiro, A. T., Barloon, P. J., & Goetz, A. F. H. (1993). The spectral image processing system (SIPS)—interactive visualization and analysis of imaging spectrometer data. *Remote Sensing of Environment*, 44(2-3), 145-163. doi:10.1016/0034-4257(93)90013-N
- Leckie, D. G., Gougeon, F. a., Tinis, S., Nelson, T., Burnett, C. N., & Paradine, D. (2005). Automated tree recognition in old growth conifer stands with high resolution digital imagery. *Remote Sensing of Environment*, 94(3), 311-326.
doi:10.1016/j.rse.2004.10.011
- Leckie, D., Gougeon, F., Hill, D., Quinn, R., Armstrong, L., & Shreenan, R. (2003). Combined high-density lidar and multispectral imagery for individual tree crown analysis, 29(5), 633-649.
- Mostafa, M. M. R. (2001). DIRECT POSITIONING AND ORIENTATION SYSTEMS HOW DO THEY WORK ? WHAT IS THE ATTAINABLE ACCURACY ? DESCRIPTION OF THE POS / AV TM DIRECT GEOREFERENCING SYSTEM Inertial Measurement Unit (IMU). In *Proceedings, American Society of Photogrammetry and Remote Sensing Annual Meeting*. St. Louis.
- Muller, R., & Lehner, M. (2002). A program for direct georeferencing of airborne and spaceborne line scanner images. In *Proceedings of the ISPRS Commission I Symposium; Integrating Remote Sensing at the Global, Regional and Local Scale*. Retrieved from <http://www.isprs.org/proceedings/XXXIV/part1/paper/00072.pdf>
- Niemann, K. O., Adams, S., & Hay, G. (1998). Automated tree crown identification using digital orthophoto mosaics. In ... *International Forum on Automated* Retrieved from <http://www.cfs.nrcan.gc.ca/pubwarehouse/pdfs/5174.pdf#page=102>

- Niemann, K. O., Frazer, G., Loos, R., & Visintini, F. (2009). LiDAR-guided analysis of airborne hyperspectral data. *2009 First Workshop on Hyperspectral Image and Signal Processing: Evolution in Remote Sensing*, 1–4. doi:10.1109/WHISPERS.2009.5289029
- Schlapfer, D., & Richter, R. (2002). Geo-atmospheric processing of airborne imaging spectrometry data. Part 1: Parametric orthorectification. *International Journal of Remote Sensing*, 23(13), 2609–2630. doi:10.1080/01431160110115825
- Sheng, Y., Gong, P., & Biging, G. (2003). True orthoimage production for forested areas from large-scale aerial photographs. *Photogrammetric Engineering and Remote ...*, 69(3), 259–266. Retrieved from http://asprs.org/a/publications/pers/2003journal/march/2003_mar_259-266.pdf
- Strahler, A. H., Woodcock, C. E., & Smith, J. a. (1986). On the nature of models in remote sensing. *Remote Sensing of Environment*, 20(2), 121–139. doi:10.1016/0034-4257(86)90018-0
- Tiede, D., Hochleitner, G., & Blaschke, T. (2005). A full GIS-based workflow for tree identification and tree crown delineation using laser scanning. In U. Stilla, F. Rottensteiner, & S. Hins (Eds.), *CMRT05, IAPRS* (Vol. 36, pp. 9–14). ISPRS.org. Retrieved from http://www.isprs.org/proceedings/xxxvi/3-w24/papers/cmrt05_tiede_et_al.pdf
- Wulder, M., Niemann, K., & Goodenough, D. (2000). Local maximum filtering for the extraction of tree locations and basal area from high spatial resolution imagery. *Remote Sensing of Environment*, 4257(00). Retrieved from <http://www.sciencedirect.com/science/article/pii/S0034425700001012>
- Yastikli, N., Toth, C., & Brzezinska, D. (2008). Multi sensor airborne systems: The potential for in situ sensor calibration. ... *Photogramm. Remote Sens. Spat. Inf. Sci.* Retrieved from <http://citeseerx.ist.psu.edu/viewdoc/download?doi=10.1.1.184.4272&rep=rep1&type=pdf>
- Yoon, J. (2008). Ortho-rectification of a Digital Aerial Image using LiDAR-derived Elevation Model in Forested Area, 24(5), 463–471.

Appendix A List of Abbreviations

Abbreviation	Definition	Page
AGL	Above Ground Level	11
AIS	Airborne Imaging Spectrometer	1
AISA	Airborne Imaging Spectrometer for Applications	12
ALS	Airborne Lidar Scanner	1
	American Society for Photogrammetric Remote	
ASPRS	Sensing	16
CCD	Charge Coupled Device	10
CHM	Canopy Height Model	5
CMOS	Complementary Metal Oxide Semiconductor	10
DBH	Diameter at Breast Height	34
DEM	Digital Elevation Model	15
DN	Digital Number	13
DSM	Digital Surface Model	2
EO	External Orientation	18
FODIS	Fiber Optic Downwelling Irradiance Sensor	12
FOV	Field of View	15
GPS	Global Positioning System	9
GSD	Ground Sampling Distance	11
H-resolution	High resolution	1
HIFOV	Horizontal Field of View	10
HLRG	Hyperspectral Lidar Research Group	38
IFOV	Instantaneous Field of View	3
IMU	Inertial Measurement Unit	10
INS	Inertial Navigation System	3
ITC	Individual Tree Crown	1
L-resolution	low resolution	1

MAP	Multiple Airborne Platforms	2
MODTRAN 5	MODerate resolution atmospheric TRANsmission	14
MRU	Motion Reference Unit	22
OBIA	Object Based Image Analysis	1
POS A/V	Position and Orientation System for Airborne Vehicles	8
SAM	Spectral Angle Mapper	40
SBET	Smoothed Best Estimate of Trajectory	19
SFRM	Strategic Forest Research Management	35
SNR	Signal to Noise Ratio	1
SOL	Start of Line	18
SV	Space Vehicle	34
SWIR	Short Wave Infrared	9
TRSI	Terra Remote Sensing Incorporated	2
VNIR	Visible Near Infrared	2